UNIVERSIDAD SAN FRANCISCO DE QUITO USFQ

Colegio de Ciencias e Ingenierías

Nanocasting of advanced $Gd_xBi_{1-x}FeO_3$ (x=0.05, 0.10, 0.15) photocatalyst for wastewater dye removal
Proyecto de Investigación
.

Sofía Carolina Andrade Tirado

Ingeniería Ambiental

Trabajo de titulación presentado como requisito
para la obtención del título de Ingeniería Ambiental

Quito, 15 de julio de 2019

UNIVERSIDAD SAN FRANCISCO DE QUITO USFQ

COLEGIO DE CIENCIAS E INGENIERÍAS

HOJA DE CALIFICACIÓN

DE TRABAJO DE TITULACIÓN

Nanocasting of advanced $Gd_xBi_{1-x}FeO_3$ (x=0.05, 0.10, 0.15) photocatalyst for wastewater dye removal

Sofía Carolina Andrade Tirado

Calificación:

Nombre del profesor, Título académico: Thomas Cadenbach, Dr. rer. nat.

Firma del profesor:

_____

Quito, 15 de julio de 2019

DERECHOS DE AUTOR

Por medio del presente documento certifico que he leído todas las Políticas y Manuales de la Universidad San Francisco de Quito USFQ, incluyendo la Política de Propiedad Intelectual USFQ, y estoy de acuerdo con su contenido, por lo que los derechos de propiedad intelectual del presente trabajo quedan sujetos a lo dispuesto en esas Políticas.

Asimismo, autorizo a la USFQ para que realice la digitalización y publicación de este trabajo en el repositorio virtual, de conformidad a lo dispuesto en el Art. 144 de la Ley Orgánica de Educación Superior.

Firma del estudiante: _____

Nombres y apellidos: Sofía Carolina Andrade Tirado

Código: 00117456

Cédula de Identidad: 1719376558

Lugar y fecha: Quito, 15 de julio de 2019

AGRADECIMIENTOS

A mis padres, Mónica y Edgar, quienes mediante sus acciones y guía me han formado como estudiante y principalmente como persona. Además de que siempre han estado pendientes de mi bienestar y felicidad. De igual forma, a mi hermana, Melissa, que siempre se ha mostrado dispuesta a ayudarme en todo ámbito.

A Thomas Cadenbach, quien desde el primer momento me permitió ingresar a su equipo de investigación, y con su paciencia y excelente disposición me guío sabiamente a lo largo de este trabajo de investigación.

A Lucía Morales y José Daza por su colaboración, buena predisposición y compañerismo durante la realización del trabajo de investigación.

A María José Benítez y Christian Santacruz del Departamento de Física de la Escuela Politécnica Nacional (EPN), así como a Alexis Debut del Laboratorio de Caracterización de Nanomateriales de la Escuela Politécnica del Ejercito (ESPE); quienes contribuyeron en la caracterización de los nanomateriales sintetizados en este proyecto.

A mis profesores y compañeros de Ingeniería Ambiental por su aporte en mi crecimiento académico y personal a lo largo de esta carrera universitaria.

De manera especial, reitero mi agradecimiento a mi papi, Edgar, quien desde temprana edad me inculcó la humildad, esfuerzo, perseverancia, autoconfianza y don de gentes.

Resumen

La presencia de colorantes en aguas residuales genera contaminación y amenaza a los diversos ecosistemas existentes, así como a los seres humanos y animales que habitan en estos; principalmente debido a su difícil degradabilidad mediante tratamientos convencionales. Es por ello, que se ha visto la necesidad de profundizar en la investigación de técnicas de oxidación avanzada, siendo la catálisis heterogénea, una de las más apropiadas. Esta técnica, a través de catalizadores produce radicales hidroxilos oxidantes que reaccionan con el colorante y generan la mineralización completa de estos contaminantes orgánicos en CO_2 y H_2O. Sin embargo, dado que la activación de los catalizadores se da mediante una fuente de energía (fotocatálisis), esta debe ser ambiental y económicamente viable; como el caso del $BiFeO_3$, cuya activación se da mediante luz visible, la cual está presente en un 48% de la luz solar. Por lo tanto, mediante este trabajo de investigación, se presentan los hallazgos relativos a la síntesis del fotocatalizador $Gd_xBi_{1-x}FeO_3$ (x=0.05, 0.10, 0.15), y cuya eficiencia fue evaluada mediante difracción de rayos X, espectrometría UV-VIS, FT IR, TEM y mediciones magnéticas.

Palabras clave: colorantes, aguas residuales, fotocatálisis, $BiFeO_3$, $BiFeO_3$ dopado, luz visible.

Abstract

The presence of dyes in wastewater generates pollution and threatens the various existing ecosystems, as well as the human beings and animals that inhabit them; mainly due to its difficult degradability by conventional treatments. That is why we have seen the need to deepen the investigation of advanced oxidation techniques, with heterogeneous catalysis being one of the most appropriate. This technique, through catalysts, produces oxidative hydroxyl radicals that react with the dye and generate the complete mineralization of these organic pollutants in CO_2 and H_2O. However, since the activation of the catalysts is through an energy source (photocatalysis), it must be environmentally and economically viable; as the case of $BiFeO_3$, whose activation is given by visible light, which is present in 48% of sunlight. Therefore, through this research work, we present the findings related to the synthesis of $Gd_xBi_{1-x}FeO_3$ (x=0.05, 0.10, 0.15) photocatalyst, and which efficiency was evaluated by X-ray diffraction, UV-VIS and FT IR spectrometry, TEM and magnetic measurements.

Keywords: Dyes, wastewater, photocatalysis, $BiFeO_3$, doped $BiFeO_3$, visible light.

General index content

Table index

Figure index

1. Introduction

"Water is not a commercial product like any other but, rather, a heritage which must be protected, defended and treated as such"- (European Commission, 2000).

Rapid population growth of approximately 7.7 billion people (World Population Review, 2019) has induced a six-fold increase in freshwater withdrawals since 1900 (Ritchie & Roser, 2019) and in the last 50 years, this amount has tripled (Worldometers, 2019). However, this will be even more complicated considering that it has been projected that water demand will increase much faster, especially in industrial and domestic sectors, and in a lower, but important degree, in the agricultural one (WWAP, 2018); where the global average is 70 percent of currently freshwater withdrawals (Ritchie & Roser, 2019).

Despite this, it is increasingly difficult to provide high-quality water, considering its global impacts due to the nutrient load associated with pathogens and the presence of hundreds of chemical products (WWAP, 2018), such as those from wastewater discharges of dyes and pharmaceutics.

Dye discharges compared with medicine water release (and its related areas), have highest values for pH, conductivity, DO, TDS, COD and BOD (Aneyo et al., 2016). Additionally, due to their complex molecular structure, synthetic origin, high color intensity, and toxicity, they are difficult to degrade (Nasar & Mashkoor, 2019) by biological or traditional physicochemical treatments, like coagulation and flocculation or adsorption (Masi et al., 2019).

All dye molecules have in common two main components responsible for imparting color (chromophore) and improving color attraction (auxochrome) (Nasar & Mashkoor, 2019). Chromophore A chromophore has a conjugated double bond that absorbs electromagnetic

radiation in the visible region, while an auxochrome is a functional group of atoms which modifies the wavelength absorption capacity of the chromophore, that is attached to it (Gürses, Akın & Özgür, 2016). Nevertheless, due to the great diversity of dyes, they can be classified based on their source (natural or synthetic), chromophore group (acridine, azo, nitroso, indophenol, anthraquinone, arylmethane or xanthene dyes) or substrate application (acid, basic, azoic, sulfur, solvent, reactive, etc.) (Nasar & Shakoor, 2017).

Specifically, due to colorfastness and low cost of Rhodamine B (RhB) (Khani Sobhani & Yari, 2019), it is intensively use in plastic, paper, leather, textile, and even food industry (to improve products aspect). However, it must be considered that since 1987 the International Agency for Research on Cancer (IARC) classified it as part of Group 3, implying that it is unknown its carcinogenic potential, so there is not overall safety among its use (IARC, 2019). For instance, it generates irritation of the respiratory tract, eyes, and skin; as experimentally it has been proven the carcinogenicity, reproductive, neuro, and chronic toxicity if swallowed by animals and human beings (Jain et al., 2007). Therefore, this has led to worldwide efforts to limit exposure of organisms to RhB and other dyes by applying alternative methods like chemical oxidation or advanced oxidation processes, such as photocatalysis.

The mechanism of photocatalysis is developed due to two key pieces: energy sources (like sunlight or UV light) and environmentally friendly semiconductors; which contribute to the degradation of dyes present in water (Jiao et al., 2018). As Figure 1 shows, photocatalytic reactions start when the catalyst absorbs a photon that has higher energy than its band gap, producing the activation of its electrons (e-) by moving it from the valence band to the conduction band, where holes (h+) are formed. The reaction of H_2O at these (h+) results in the production of OH* (hydroxyl radicals). These radicals will react with dyes and degrade it producing CO_2 and H_2O (Emy Marlina et al., 2015).

At the same time, the (e-) of the conduction band react with the dissolved oxygen species forming superoxide ions, which are attached to intermediate products and form hydrogen peroxide that is transformed into H_2O (Saravanan et al., 2017).
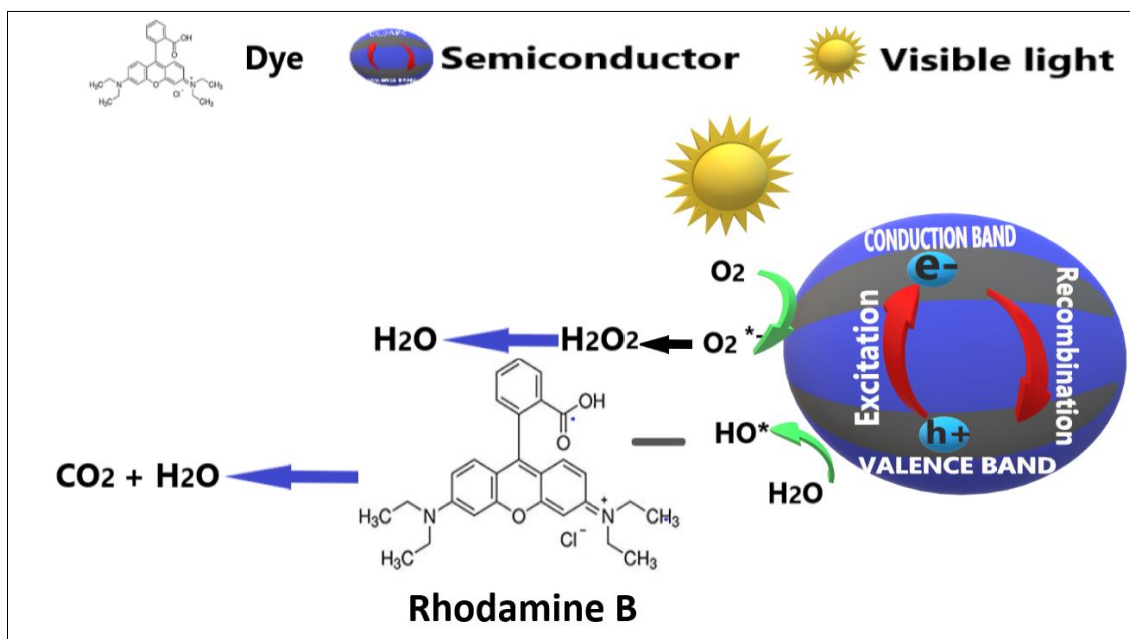
Figure 1. Photocatalysis mechanism for the degradation of dyes

However, it is important to consider, that the photocatalytic capacity is limited by the recombination of (e-) on (h+), in which the absorbed light is released as heat, the OH* are not produced and the degradation does not take place (Ibhadon & Fitzpatrick, 2013).

Among pioneer photocatalytic materials, it has been proven that TiO_2, ZnO, and SnO_2 present robust chemical stability, nontoxicity and high reactivity (Bai, 2016). However, their applications are limited due to their wide bandgap bigger than 3 eV, i.e. it can just be activated under ultraviolet irradiation, which range of the spectrum is between 100-400nm. Therefore, the access to it can be by natural sources, taking just 5% of sunlight, or artificial sources, like fluorescent lamps, gas-discharge lamps, laser and LED lights (Tamuri et al., 2014). Due to this, efforts have been focusing on developing

photocatalysts that require less artificial energy and increases the use of visible light (380nm<λ<750nm).

Fortunately, in the last years $BiFeO_3$ has been discovered as promising material, that in comparison with other semiconductors, has a short band gap value between 2-2.8 eV. This gives larger photon efficiency and enhanced interaction between its electrons and holes, allowing to benefit from a wider part of the sunlight spectrum and ensuring a greater separation of the photogenerated charge carriers (Bai, 2016).

However, it has been seen that pure $BiFeO_3$ has a low conduction band position in comparison to the oxygen reduction level (Humayun et al., 2016). Therefore, in order to make $BiFeO_3$ an ideal photocatalyst that develops efficiently oxidation-reduction processes for dye decomposition, it is required to expand its surface area and thus its reactivity (Bai, 2016). This can be achieved by replacing in a certain degree Bi^{3+} ions with rare-earth elements (La^{3+}, Nd^{3+}, Sm^{3+} or Gd^{3+}), which also will delay recombination of (e-) on (h+), facilitate specific reactions on the photocatalysts surface, broaden the absorption spectrum and increase photo-stability (Gebreslassie et al., 2013).

In comparison with the other chemicals, the use of Gadolinium (Gd) for doping $BiFeO_3$ has display desirable photocatalytic advantages as it generates more surface defects, that could capture the photo-induced (e-) to further produce excitons. This has been demonstrated by advanced techniques related to the recombination of excited (e-) and (h+), like photoelectrochemical, photocurrent and electrochemical impedance spectra measurements, in which 1-5% Gd-$BiFeO_3$ samples were able to capture photoinduced (e-) in a better way than pure $BiFeO_3$ due to a reduction in the photoelectrochemical intensity (Zhang et al., 2016).

However, by the analysis of XRD Patterns, it has been probed that photocatalytic activity decreases with a further increase of Gd. For example, samples doped with 20% of Gd, synthesized by a wet chemical method exhibit a distorted structure, implying that the solubility limit is achieved doping with 10% of Gd (Yanoh et al., 2014). Similarly, samples obtained by a sol-gel procedure, doped with Gd until 10% conserve a rhombohedral structure in comparison with the ones doped with 5,10 and 15%, (Guo et al., 2010).

Likewise, using the sol-gel technique, 1,3,5% Gd- $BiFeO_3$ and pure $BiFeO_3$ samples were compared, and 3% Gd-$BiFeO_3$ exhibits 2.55 times more degradation efficiency, as well as a low emission intensity, indicating a decrease in recombination probability of excited (e-) and (h+) (Zhang et al., 2016). Similarly, in other experiments, samples doped with 4,8 and 12% of Gd were analyzed using TEM images and 12% Gd-$BiFeO_3$ sample showed nanoparticles well-dispersed, without aggregation, spherical symmetry and homogenous in size of 26nm (Lotey & Verma, 2013).

Specifically, the mechanism to improve photocatalytic activity during the degradation of dyes, like RhB, starts when Gd-doped $BiFeO_3$ particles are excited by visible light ($\lambda \geq 420$ nm) to produce photogenerated electrons (e-) and holes (h+) (Eq. 1). Gd traps those excited (e-) (Eq. 2) and facilitates the separation of electron-hole pairs, promoting the charge transfer from the bulk $BiFeO_3$ to the surface of the photocatalyst. Therefore, the photoinduced electrons transferred from the Gd dopant to the photocatalyst surface could capture the adsorbed O_2 and reduce it to O_2^{*-} (Eq. 3). The photogenerated (h+) once transported to the photocatalyst surface could also react with H_2O to form $\cdot$ OH (Eq. 4) to directly oxidize RhB (Eq. 5) or degrade it (Eq. 7). Apart from $\cdot$ OH, in the degradation process, (h+) and superoxide radicals are also the reactive species for RhB degradation (Eqs. 5 and 6), while hydroxyl radicals could also play a minor role (Eq. 7) (Zhang, 2016).

$$Bi_{(1-x)}Gd_{(x)}FeO_3 + h\nu \rightarrow e^- + h^+ \qquad (1)$$

$$e^- + Gd\ dopant \rightarrow e^-\ (Gd\ dopant\ trapped) \quad (2)$$

$$e^-(Gd\ dopant\ trapped) + O_2 \rightarrow O_2^{*-} \qquad (3)$$

$$h^+ + H_2O \rightarrow \cdot OH \qquad (4)$$

$$h^+ + RhB \rightarrow degradation\ products \qquad (5)$$

$$O_2^{*-} + RhB \rightarrow degradation\ products \qquad (6)$$

$$\cdot OH + RhB \rightarrow degradation\ products \qquad (7)$$
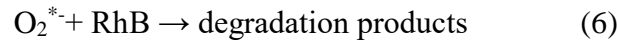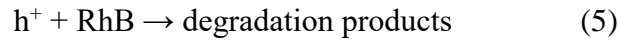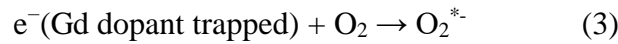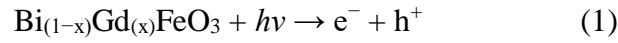
In order to achieve a higher photocatalytic activity, it is essential to consider the catalyst structure and size. Ideally, nanomaterials are expected as it is known that they have large surface areas and band gaps of around 2.3 eV, in comparison to bulk (large) materials that have band gaps bigger than 3 eV. Likewise, when the size of the catalysts is smaller, more atoms are accumulated on the surface leading to an increase in the surface to volume ratio (Saravanan et al., 2017). This property increases the number of active sites (Saravanan et al., 2017), resulting in faster dye degradation as it can be generated by more $\cdot$OH radicals. Therefore, due to these requirements, ordered mesoporous materials are desirable as they have a high surface area, manageable pore size and good chemical/thermal stability of the rigid framework over conventional bulk and nanoparticle counterparts (Deng, Chen & Tüysüz, 2016).

Concretely, as it has been described before, Gd doped $BiFeO_3$ has a great potential to enhance the photocatalytic activity during the degradation of dyes, and that is why, the aim of this work is to develop soft templating and hard templating (nanocasting) techniques for obtaining $Gd_xBi_{1-x}FeO_3$ (x=0.05, 0.10, 0.15) nanomaterials as photocatalysts.

Soft templating materials are obtained by a self-assembly process induced by surfactants or block copolymers, like Pluronic 123 (P123, Polyethylene glycol-Poly propylene

glycol-Poly ethylene glycol) that acts as the structure-directing agent (Deng, Chen & Tüysüz, 2016). It implies complex sol-gel interactions between chemical and surfactant species to form determined structures, which essentially depend on concentration, pH and solvents. Once the structures are formed, the complexes of the precursors are collocated around acquiring the shape of the structure; and by calcination processes, it is possible to obtain the desired materials in the shape of the initial copolymers (see Figure 1.1).
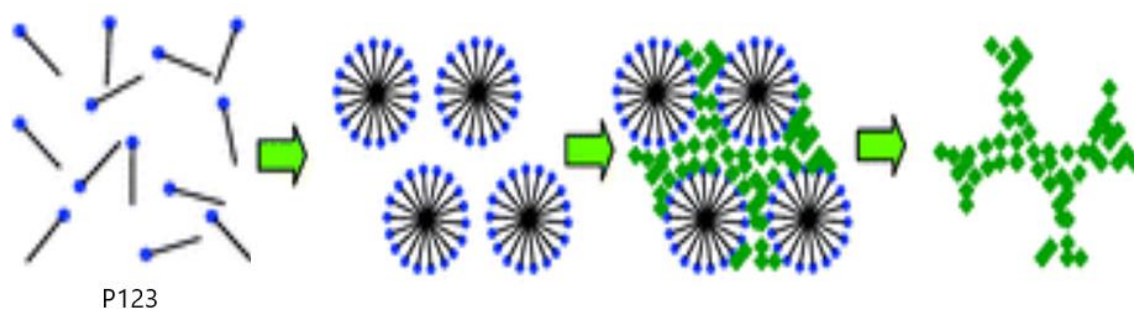
Figure 1.1. Soft templating process

For the hard templating processes, SBA-15 and KIT-6 (in preliminary experiments) were used, as both display a two-dimensional hexagonal order, in which SBA-15 has p6mm symmetry (Zhao et al., 1998) and KIT-6 an Ia3d symmetry with two interpenetrating bi-continuous mesopore systems (Kleitz, Choi & Ryoo, 2003). They are obtained in a similar way, except for the addition of butanol to KIT-6, as it requires another decisive directing agent for the cubic phase formation (Deng, Chen & Tüysüz, 2016). These templates are hard mesoporous SiO_2 with a pore size between 2-50 nm were the resulting replica morphology is independent of pH, concentration, and solvents. As it can be seen in Figure 1.2, the templating reagents are infiltrated with the precursors of the desired product and after the evaporation of solvents, the pores are either partially or completely filled (Deng, Chen & Tüysüz, 2016). Subsequently, by leaching with NaOH, the silica templates are

removed, and depending on the techniques used to fill the material, there are obtained the liberated particles or wires.
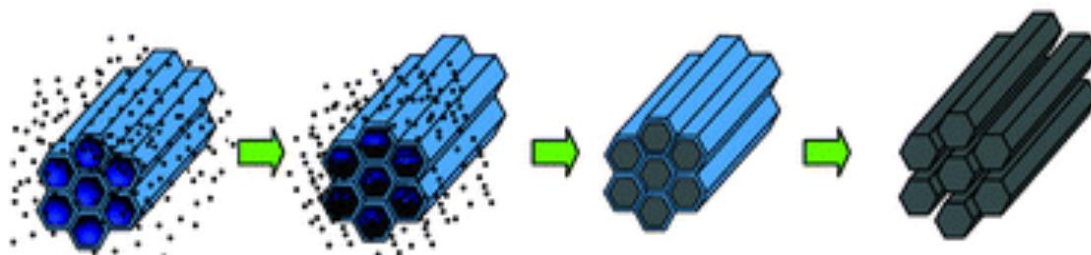
Figure 1.2. Hard templating process

Regarding the synthesis of the catalysts, due to heat, it occurs the decomposition of NO_x (essentially NO and NO_2) and CO_2, which come from the precursors and Tartaric acid - TA [$C_4H_6O_6$], respectively providing the needed space for new $Bi(NO_3)_3$ and $Fe(NO_3)_3$. However, it is imperative to use the precursors in stoichiometrically proportions, in order to avoid deviations or impurities from the starting compounds, which leads to the formation of secondary phases like the mullite phase ($Bi_2Fe_4O_9$) or a sillenite type phase ($Bi_{25}FeO_4$) (Lahmar, 2011).

Additionally, depending on the developed procedure, TA is used as a chelating agent, as it complexes the metal cations of the precursors, avoiding the formation of precipitates before evaporation (Mukherjee, 2014). The orientation of its two hydroxyls and two carboxylate groups creates heterometallic polynuclear complexes in the solution, which lead to the bismuth ferrite formation upon calcination (Ghosh, 2005).

Finally, the synthesized $Gd_xBi_{1-x}FeO_3$ (x=0.05, 0.10, 0.15) nanomaterials are analyzed by X-ray diffraction (XRD), transmission electron microscopy (TEM), UV-Vis diffuse reflectance spectroscopy and FT IR spectra measurements. Moreover, the photocatalytic activities are analyzed by the degradation of the dye RhB at room temperature under

visible-light irradiation; in which the chosen dye with an isolated band at around 555 nm makes it relatively easy the interpretation of the UV-Vis spectra (Santillán, 2017).

2. Experimental description

2.1. Characterization techniques and equipment

The crystalline structure of all the synthesized nanomaterials and silica templates were examined by X-ray diffraction (XRD) using a PANalytical Empyrean diffractometer that has a 2θ configuration with a Cu-tube of 1.54Å and a XCELERATOR detector; as well as a Bruker D2 Phaser with a Cu-tube of 1.54Å and a LYNXEYE XE-T detector. The samples impurities were identified by Match! 3 – Phase Identification from Powder Diffraction.

For the samples that required the analysis of its morphology, the transmission electron microscopy (TEM) images were obtained by a FEI Tecnai G2 spirit twin transmission electron microscope.

By a Perkin Elmer UV-Vis spectrometer with an integrating sphere attachment, UV-Vis diffuse reflectance spectra of the nanomaterials were measured. The obtained values of absorbance per wavelength were processed using the Kubelka-Munk method (1931), obtaining the incident light energy as a function of the Kubelka-Munk remission function by photon energy squared, and at the end, the band gap values were calculated by extrapolation of the linear plot in the abscissa axis.

Using the Jasco FT IR-4700 spectrometer Fourier transformed infrared (FT IR) spectra were obtained.

The photocatalytic activity measurements of the absorption spectrum of RhB was accomplished using the UV-Visible spectrophotometer Genesys 30 TM that has a Tungsten-Halogen light source and a silicon photodiode detector. This data was normalized and processed for obtaining the percentage and kinetics of degradation.

2.2. Synthesis of silica templates

2.2.1. SBA-15 & KIT-6

Components:

- Pluronic 123 (P123, Polyethylene glycol-Poly propylene glycol-Poly ethylene glycol); EO:PO: EO= 20:70:20
- HCl (37-38 %)
- 1-Butanol (99%)
- Deionized H_2O
- TEOS (tetraethyl orthosilicate) (98%)

The synthesis of SBA-15 & KIT-6 was done by slightly modifying the previous method reported by Deng and collaborators (2016).

For the obtention of 6.9g of SBA-15 with a 95% yield, 13.9g of Pluronic P123, 252ml of deionized H_2O and 6.42ml of HCl were mixed in a 100ml polypropylene container at 35°C in a water bath, until a clear solution was obtained. Then, 26.8ml of TEOS was added and the solution was stirred in the water bath for 24h at 35°C. After that, for hydrothermal treatment, the solution was dried at 100°C for 24h and by vacuum filtration, the dense precipitate was collected and dried for 24h at 100°C. Finally, the obtained powder was crushed and calcined at 550°C for 9h using a 0.9°C/min heating rate.

Similarly, in order to get 6.5g of KIT-6 with a 95% yield, 13.5g of Pluronic P123, 487.5ml of deionized H_2O and 21.75ml of HCl were mixed in a 100ml polypropylene container at 35°C in a water bath, until a clear solution was obtained. Then, as it requires another

decisive directing agent for the cubic phase formation, 13.5ml of 1-Butanol was added and, after 1h, 29ml of TEOS was added and the solution was stirred in the water bath for 24h at 35°C. Subsequently, for hydrothermal treatment, the solution was dried at 100°C for 24h and by vacuum filtration, the dense precipitate was collected and dried for 24h at 100°C. Finally, the obtained powder was crushed and calcined at 550°C for 9h using a 0.9°C/min heating rate.

2.2. Synthesis of mesoporous $Gd_xBi_{1-x}FeO_3$ (x=0.05, 0.10, 0.15) by a soft templating technique

Components:

- Bismuth nitrate $[Bi(NO_3)_3(H_2O)_5]$
- Gadolinium nitrate $[Gd(NO_3)_3(H_2O)_6]$
- Iron nitrate $[Fe(NO_3)_3(H_2O)_9]$
- P123
- Deionized H_2O
- Ethylene glycol $[C_2H_6O_2]$
- Glacial Acetic Acid $[CH_3COOH]$

Table 1. Precursors for the synthesis of $Gd_xBi_{1-x}FeO_3$ (x=0.05, 0.10, 0.15) nanoparticles via sol-gel technique

ID	Sample	Precursors (g)			P123 (g)	H₂O (ml)
		$Bi(NO_3)_3(H_2O)_5$ (g)	$Gd(NO_3)_3(H_2O)_6$ (g)	$Fe(NO_3)_3(H_2O)_9$ (g)		
D1 & D3	10%-Gd BiFeO₃	1.0809	0.1118			
	mmol	2.2283	0.2476			
D2	10%-Gd BiFeO₃	1.0782	0.11148			-
	mmol	2.2227	0.2469			
15P	15%-Gd BiFeO₃	1.01838	0.1672	1	0.07	
	mmol	2.0999	0.3704			
K	5%-Gd BiFeO₃	1.141	0.056			5
	mmol	2.352	0.124			277.77
X		1.141	0.056			-

L	5%-Gd BiFeO$_3$				
G	5%-Gd BiFeO$_3$				0.14
H	H:5%-Gd BiFeO$_3$				0.28
I	5%-Gd BiFeO$_3$				0.56
	mmol	2.352	0.124	2.47	

The precursors were mixed at room temperature (RT) according to Table 1, dissolving them in 24.76ml of ethylene glycol and H$_2$O (only for sample K). After 30min, 24.76ml of glacial acetic acid was added and after 30min Pluronic P123 was added and the solution was stirred at 50°C for 2h. Subsequently, the solution was dried at 80°C for 12h until a gel was obtained and finally, it was calcined at 450°C for 1h30 using a 1°C/min heating rate.

2.3. Synthesis of mesoporous Gd$_x$Bi$_{1-x}$FeO$_3$ (x=0.05, 0.10, 0.15) by hard templating techniques

2.3.1. Two-step impregnation technique

2.3.1.1. Experiment 1

Components:

- Bismuth nitrate [Bi(NO$_3$)$_3$(H$_2$O)$_5$]
- Iron nitrate [Fe(NO$_3$)$_3$(H$_2$O)$_9$]
- Tartaric acid - TA [C$_4$H$_6$O$_6$]
- 2-Methoxyethanol [C$_3$H$_8$O$_2$]
- Nitric acid [HNO$_3$]

Table 2. Precursors for the synthesis of BiFeO$_3$ by the 2-step impregnation process

Mixture	Precursors (g)		TA (g)
	Bi(NO$_3$)$_3$(H$_2$O)$_5$	Fe(NO$_3$)$_3$(H$_2$O)$_9$	C$_4$H$_6$O$_6$
1: 60%	2.9177	2.43	0.9027
mmol	6.015	6.015	6.015
2: 40%	1.9451	1.6199	0.6018
mmol	4.0099	4.0099	4.0099

According to quantities of Table 2, in two individual beakers (by duplicate), the precursors were mixed and dissolved taking 30ml of a solvent solution (60ml of 2-methoxyethanol and 30ml of nitric acid [2M]). After 30min TA was added and after 1h of stirring, once the solution was clear, 2.156g of KIT-6 were added and the solution was left stirring overnight. Then, using a rotavap at 80°C, the solvent was extracted and it was obtained a powder that later was dried in the oven at 70°C for 3h.

For the first impregnation, duplicates were weighed and separated each one into two beakers, obtaining four samples that were individually heated according to Table 3.

Table 3. Heating temperature and time for the 2-step synthesis of BiFeO$_3$

ID	Sample	Temperature (°C)	Time (h)	Heating rate (°Cmin^{-1})
SA1		200		
SA2	BiFeO$_3$	300	3	4
SA3		350		
SA4		450	2	

Afterwards, the precursors of the mixture 2 presented in Table 2 were dissolved using 30ml of a solvent solution (60ml of 2-methoxyethanol and 30ml of nitric acid [2M]). Then, TA was added and the solution was left stirring at RT for 1h. To each of the 4 samples obtained during the first impregnation process, 10ml of mixture 2 was added and they were left stirring overnight. After this, in the rotavap at 80°C the solvent was extracted, obtaining powders that were dried in the oven at 70°C for 3h.

Finally, for the second impregnation, the four samples were heated individually according to Table 3 and in the same heating process, they were additionally calcined at 500°C for 1h.

2.3.2. Combustion technique

2.3.2.1. Experiment 1

Components:

- Bismuth nitrate [$Bi(NO_3)_3(H_2O)_5$]
- Iron nitrate [$Fe(NO_3)_3(H_2O)_9$]
- Tartaric acid - TA [$C_4H_6O_6$]
- Nitric acid [HNO_3]

Table 4. Precursors for the synthesis of $BiFeO_3$ in the first experiment of the combustion technique

Sample	Precursors (g)		TA (g)
	$Bi(NO_3)_3(H_2O)_5$	$Fe(NO_3)_3(H_2O)_9$	$C_4H_6O_6$
$BiFeO_3$	1.6322	1	1.2404
mmol	3.3648	2.4752	8.2645

Based on quantities of Table 4, in two individual beakers (by duplicate) the precursors were mixed and dissolved in 24.76ml of nitric acid [2M]. After stirring the solution at RT for 30min, TA was added and it was left stirring for 30min more. Then, the solution was stirred at 150°C until the solvent was completely evaporated. Finally, the powders obtained by duplicate were individually calcined at 450°C and 500°C for 2h at 4°C/min.

2.3.2.2. Experiment 2

Components:

- Bismuth nitrate [$Bi(NO_3)_3(H_2O)_5$]
- Iron nitrate [$Fe(NO_3)_3(H_2O)_9$]

- Tartaric acid - TA [$C_4H_6O_6$]
- Nitric acid [HNO3]
- Deionized H_2O
- 3-aminopropanoic acid - 3-APA [$C_3H_7NO_2$]

Table 5. Precursors for the synthesis of $BiFeO_3$ nanoparticle assemblies (MBFAS) in

the second experiment of the combustion technique

Sample	Precursors (g)		TA (g)
	$Bi(NO_3)_3(H_2O)_5$	$Fe(NO_3)_3(H_2O)_9$	$C_4H_6O_6$
$BiFeO_3$	1.945	1.6199	0.602
mmol	4.0097	4..0097	4..0097

According to Table 5, the precursors were mixed and dissolved in 20ml of nitric acid

[2M], and after 30min, TA was added. Then, the solution was stirred at 150°C until the

solvent was evaporated and the obtained powder was dried at 300°C for 2h using a

4°C/min heating rate.

The obtained $BiFeO_3$ NPs were added to deionized H_2O that contains 0.3122g of 3-APA,

and the pH was adjusted to 4 using nitric acid [1M]. After leaving the mixture stirring at

RT for 48h, it was washed with deionized H_2O and centrifuged until a pH of 7 was

reached. Then, the sample was dried at 80°C and dispersed in deionized H_2O to obtain a

colloidal solution.

Afterwards, to 2ml of the obtained solution at RT for 2h, 0.14g of Pluronic P123 were

added and then the solution was dried at 40°C until a gel was formed. Finally, the sample

was calcined at 360°C for 6h using a 0.5°C/min heating rate.

2.3.3. Complexation technique

2.3.3.1. Experiment 1

Components:

- Bismuth nitrate [$Bi(NO_3)_3(H_2O)_5$]
- Iron nitrate [$Fe(NO_3)_3(H_2O)_9$]
- Tartaric acid - TA [$C_4H_6O_6$]
- 2-Methoxyethanol [$C_3H_8O_2$]
- Nitric acid [HNO_3]

Table 6. Precursors for the synthesis of BiFeO3 under evaporation of solvents without heating

Sample	Precursors (g)		TA (g)
	$Bi(NO_3)_3(H_2O)_5$	$Fe(NO_3)_3(H_2O)_9$	$C_4H_6O_6$
$BiFeO_3$	1.95	1.58	0.5868
mmol	4.02	3.91	3.91

According to Table 6, the precursors (with 2.74% of Bismuth excess) were mixed and dissolved in 40ml of 2-methoxyethanol. After 30min, TA and 4ml of nitric acid [2M] were added. Then after leaving the solution stirring at RT for 30min, 1g of mesoporous silica (SBA-15) was added. Afterwards, the solvent was extracted leaving the solution stirring at RT for 29 days and the obtained powder was calcined considering the calcination path of Figure 2.
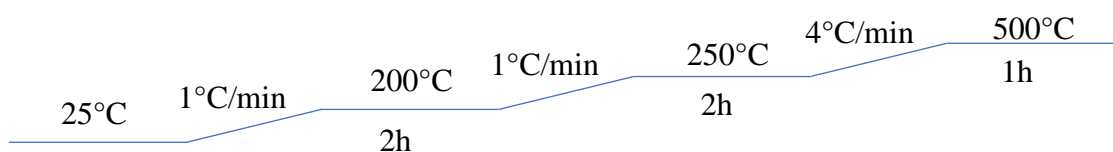
Figure 2. Calcination path for the synthesis of BiFeO$_3$ by the first experiment of the complexation technique

2.3.3.2. Experiment 2

Components:

- Bismuth nitrate [$Bi(NO_3)_3(H_2O)_5$]
- Gadolinium nitrate [$Gd(NO_3)_3(H_2O)_6$]
- Iron nitrate [$Fe(NO_3)_3(H_2O)_9$]
- Tartaric acid - TA [$C_4H_6O_6$]

- 2-Methoxyethanol [$C_3H_8O_2$]
- Nitric acid [HNO_3]

Table 7. Precursors for the synthesis of $Gd_xBi_{1-x}FeO_3$ (x=0.05, 0.10) by the

complexation technique

ID	Sample	Precursors (g)			TA (g)
		$Bi(NO_3)_3(H_2O)_5$	$Gd(NO_3)_3(H_2O)_6$	$Fe(NO_3)_3(H_2O)_9$	$C_4H_6O_6$
Gd1	5%-Gd BiFeO$_3$	1.197	0.058	1.0148	0.3770
	mmol	2.4676	0.1285	2.5118	2.5118
Gd2	10%-Gd BiFeO$_3$	1.139	0.116	1.0148	0.3770
	mmol	2.3481	0.257	2.5118	2.5118
5L	5%-Gd BiFeO$_3$	1.1576	0.0567	1.0148	0.3770
	mmol	2.3864	0.1256	2.512	2.512
10LA & 10LB	10%-Gd BiFeO$_3$	1.0966	0.1134	1.0148	0.3770
	mmol	2.2608	0.2512	2.512	2.512

Based on the quantities of Table 7, the precursors were mixed and dissolved in 30ml of 2-methoxyethanol and 15 of nitric acid [2M], with exception of sample 10LA where it was used half of each of the solvents. After 30min TA was added and the solution was stirred at RT until it was clear and once this occurred, 0.7631g of mesoporous silica (SBA-15) were added and the solution was left stirring overnight. Then, the solvent was extracted using a rotavap at 80°C and the obtained powder was dried for 3h at 75°C. Finally, the sample was calcined considering the calcination path of Figure 2.

2.3.4. One-step impregnation technique

2.3.4.1. Experiment 1

Components:

- Bismuth nitrate [$Bi(NO_3)_3(H_2O)_5$]
- Gadolinium nitrate [$Gd(NO_3)_3(H_2O)_6$]

- Iron nitrate [$Fe(NO_3)_3(H_2O)_9$]
- Tartaric acid - TA [$C_4H_6O_6$]
- Nitric acid [HNO_3]

Table 8. Precursors for the synthesis of ordered mesoporous BiFeO3 and

$Gd_{0.05}Bi_{0.95}FeO_3$ varying SBA-15 amounts

ID	Sample	Precursors (g)			TA (g)	SBA-15 (g)
		$Bi(NO_3)_3(H_2O)_5$	$Gd(NO_3)_3(H_2O)_6$	$Fe(NO_3)_3(H_2O)_9$	$C_4H_6O_6$	
SA						0.075
SB	BiFeO$_3$	0.97	-	0.8079	0.3001	0.15
SC						0.3
SD					-	0.15
	mmol	1.999	-	1.999	1.999	
SE	5%-Gd	0.9216	0.0451	0.8079	0.3001	0.15
SF	BiFeO$_3$					1.5
	mmol	1.8999	0.0999	1.999	1.999	
SY	5%-Gd	0.9212	0.045	0.8079	0.3001	0.075
SZ	BiFeO$_3$					0.3
	mmol	1.8990	0.099	1.999	1.999	
P1	BiFeO$_3$	1.2184	-	1.0148	0.3726	0.763
	mmol	2.5118	-	2.5118	2.4285	
P2	5%-Gd	1.1574	0.05678	1.0148	0.3726	0.763
P3	BiFeO$_3$					1.144
	mmol	2.3860	0.1258	2.5118	2.4825	

The precursors were mixed according to Table 8 and were dissolved in 10ml of nitric acid [2M]. Then, with the exception of SD, after 10 minutes, TA was added and the samples were stirred at RT until a clear solution was obtained. At this point, the samples were transferred to plastic containers and SBA-15 was added. After 30 min, the samples were dried at 70°C for 24h and at the end, they were calcined for 1h at 500°C using 4°C/min as heating rate.

2.3.4.2. Experiment 2

Components:

- Bismuth nitrate [$Bi(NO_3)_3(H_2O)_5$]
- Iron nitrate [$Fe(NO_3)_3(H_2O)_9$]
- Tartaric acid - TA [$C_4H_6O_6$]

- 2-Methoxyethanol [$C_3H_8O_2$]

Table 9. Precursors for the synthesis of $BiFeO_3$ under reflux condensation in the second solvent extraction

Sample	Precursors (g)		TA (g)
	$Bi(NO_3)_3(H_2O)_5$	$Fe(NO_3)_3(H_2O)_9$	$C_4H_6O_6$
$BiFeO_3$	1.37	1.13	0.4197
mmol	2.8243	2.797	2.79

Table 10. Ratio SBA-15/ $BiFeO_3$

ID	Synthesized powders		Ratio
	$BiFeO_3$ (g)	SBA-15 (g)	SBA-15:$BiFeO_3$
R, AR & BR	0.1	1	10:1
3R	1.1671	3.5013	3:1
UPS	≈1.5	1	≈ 2:3

According to Table 9, the precursors (with 0.97% of Bismuth excess) were mixed and dissolved in 30ml of 2-methoxyethanol. After 30min, TA was added and the solution was left stirring for 12h. Then, the solvent was extracted in a rotavap at 80°C and the obtained powder was collocated in the oven at 50°C until it was completely dried. Then, the obtained powder was mixed with mesoporous silica (SBA-15) in 10ml of hexane according to the ratios of Table 10. Then, the mixture was refluxed in 30ml of hexane, for 24h. The solvent was extracted in the rotavap at 69°C and at the end, it was completely dried in the oven at 50°C, the powder was calcined considering the calcination path of Figure 3.
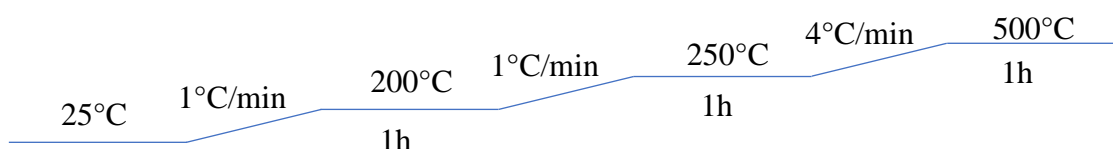
Figure 3. Calcination path for the synthesis of $BiFeO_3$ by one-step impregnation technique using hexane

2.4. Leaching process with NaOH of the synthesized materials by hard templating techniques

Components:

- Synthesized nanomaterials
- Sodium hydroxide [NaOH]

In order to liberate the nanomaterials of $Gd_xBi_{1-x}FeO_3$ (x=0.05, 0.10, 0.15) synthesized by hard templating techniques, the silica template was removed by a two-step leaching process using an excess volume of 2M NaOH and subsequent heating temperature of 70°C.

The synthesized catalysts were collocated in plastic containers and the Sodium hydroxide [2M] was added according to the calculated quantity obtained by Eq. 8. After leaving the samples in the oven at 70°C for 12h, the decanted solution was removed and the calculated amount of Sodium hydroxide [2M] was added for a second time and it was left at the previous temperature for the same period of time. Afterwards, the material was washed with deionized water and centrifuged at 4000rpm for periods of 5min, until the effluent had an approximate pH of 7. Then, the leached sample was left in the oven at 70°C until it was completely dried (Deng et al., 2016).

$$SiO_2 + 2NaOH \rightarrow Na_2SiO_3 + H_2O \quad (8)$$

2.5. Photocatalytic activity

By means of a photoreactor that irradiates visible-light, the photocatalytic activities of all the samples synthesized by soft and hard templating techniques were analyzed; which allows the identification of the degree of RhB degradation at room temperature.

Specifically, it was used a self-constructed water and air cooled photoreactor, as it is shown in Figure 4, that has high-intensity LEDs for the simulation of sunlight in the spectra of 400-700 nm.
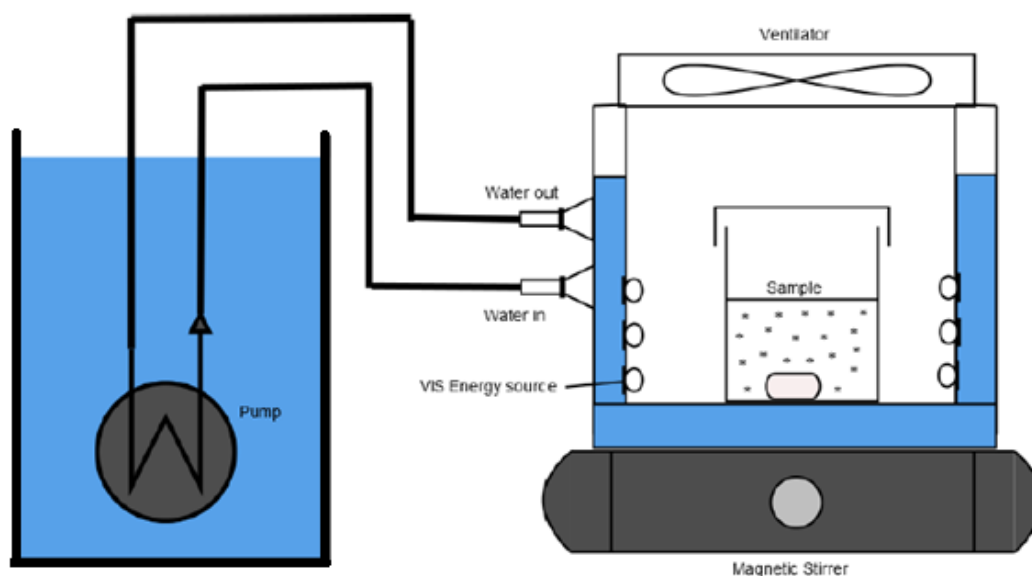
Figure 4. Experimental setup of a photoreactor

(Santillán, 2017).

In 50mL of RhB (5mg/L), 50mg of each of the catalysts were added and to achieve the adsorption-desorption equilibrium between both components, the solution was left stirring in darkness for 1h. After this, a sample was taken and the solution was exposed to visible-light irradiation for 240 min. During that period samples were then every 30min.

Once each sample was taken, by centrifugation at 4000 rpm for 5 min, the catalyst was separated from the solution and using a UV-Visible spectrophotometer, the absorption spectrum of RhB was measured. Then, for obtaining the values of concentration through time, it was considered the Beer-Lambert law (Eq. 9), in which the absorption of light by the sample (A) is defined by the incident light intensity (Io) and the transmitted intensity (I). This is equivalent to the wavelength molar absorptivity coefficient in $M^{-1}cm^{-1}$ (ε)

multiplied by the path length in cm (*l*) and the sample concentration in M (*c*) (Bai et al., 2016).

$$A = \log_{10} \frac{I_0}{I} = \varepsilon l c \quad (9)$$

Considering the previous equation, a calibration curve of RhB with R^2 of 0.9959 was obtained. Using this curve and the maximum absorption peak of each sample (obtained after linearization), the final RhB concentration was obtained.

Additionally, the kinetics of the photocatalytic degradation of the RhB solution with each of the catalysts were obtained by the Langmuir Hinshelwood expression (Eq. 10), where C_o and C are the concentrations of RhB, respectively at irradiation times t_o and t, and *k* (min^{-1}) is the pseudo first-order rate constant (Soltani & Enterazi, 2013) that is followed by the diluted RhB solution.

$$ln \frac{C}{C_0} = -kt \quad (10)$$

3. Results and discussion

3.1. Characterization of SBA-15

3.1.1. XRD measurements for the structure analysis

Following the procedure for the synthesis of SBA-15 described in the experimental description, the diffractogram showed in Figure 5 was obtained in which it is possible to see that samples synthesized in different dates have peaks between 1-2° of the diffraction angle that corresponds to a typical ordered SBA-15 with an expected p6mm symmetry (Zhao et al., 1998).
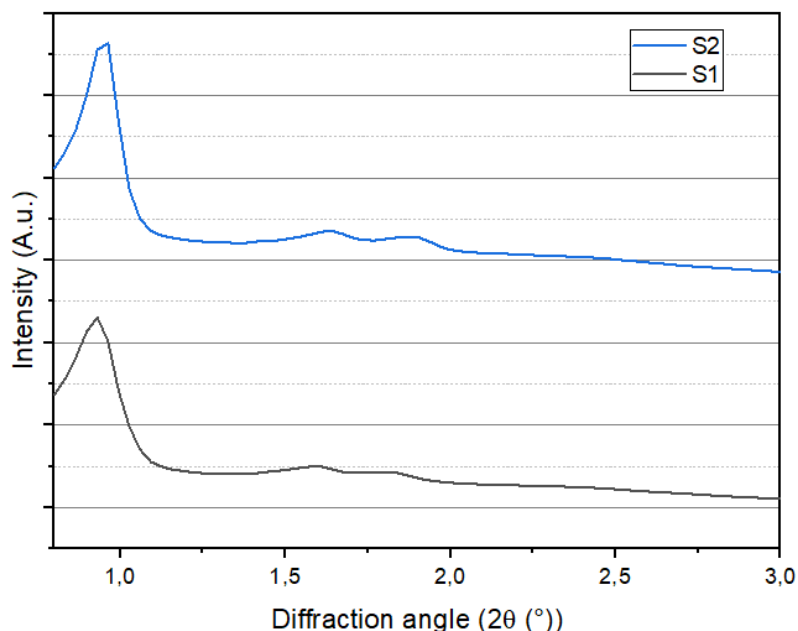
Figure 5. XRD for the synthesized SBA-15 samples

These results imply that all the components used during the synthesis display a key role. P123 acts as the structure directing agent, TEOS influences the interaction of the silicate ions oligomers with surfactant, resulting in rod-like micelles, in which the packing of the rod-like silica coated micelles provides the hexagonal phase, and therefore silica walls are formed through the hydrolysis and polymerization of TEOS (Deng et al, 2016).

Therefore, as the silica SBA-15 was successfully obtained, it was used in the procedures of all the hard templating techniques.

3.2. Characterization of mesoporous $Gd_xBi_{1-x}FeO_3$ (x=0.05, 0.10, 0.15) synthesized by a soft templating technique

3.2.1. XRD measurements for the structure analysis

The results exposed by Figure 6 indicate that the synthesis of 5%Gd-BiFeO₃ varying the P123 ratios, exhibit a similar orthorhombic structure on the XRD zooms from 30-35° of diffraction angle 2θ, with exception of the sample synthesized using 0.07g of P123, but

in the sample that additionally was collocated 5ml of H_2O, it does exhibit the same structure as the other samples.
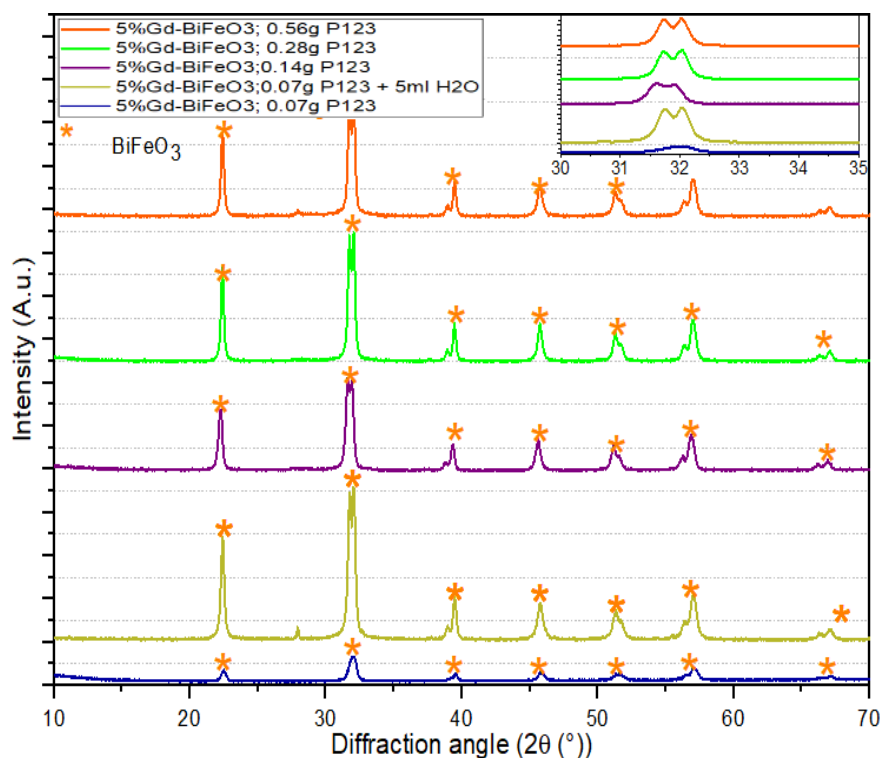
Figure 6. XRD of the synthesized $Gd_{0.05}Bi_{0.95}FeO_3$ varying from 0.07-0.56g the amount of P123

These findings suggest that P123 excess has no negative impact on the compound's purity and in fact, the solvents favorably influence the formation of nanomaterials free of undesirable bismuth oxides. In this process, ethylene glycol also acts as a surfactant that influences the size uniformity of the target material, decreasing the agglomeration degree of the distributed sphere nanoparticles (Hai et al., 2017), while glacial acetic acid acts as a stabilizer that prevents sedimentation of the precursors, as well as, hydrolysis (Song, et al., 2009).

Additionally, considering Figure 7, it is visible that the synthesized 5%,10%, and 15%Gd-BiFeO$_3$ have a similar rhombohedral structure on the peak from 31-33° of diffraction angle 2θ, which corresponds to pure BiFeO$_3$. Therefore, this implies that there is no influence of doping in the compound structure. However, considering that 15%Gd-BiFeO$_3$ exhibits the formation of Bi$_2$O$_3$ between 25-30° of diffraction angle 2θ, it suggests that doping BiFeO$_3$ with 5% and 10% of Gd is enough in order to avoid alterations on the material purity.
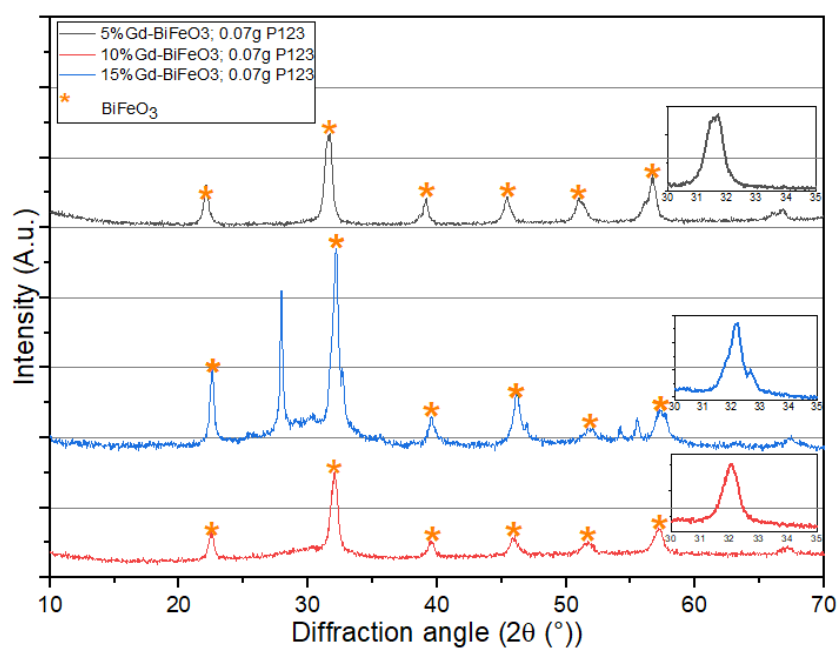
Figure 7. XRD of the synthesized Gd$_x$Bi$_{1-x}$FeO$_3$ (x=0.05, 0.10, 0.15) using 0.07g of P123

3.2.2. UV-Vis measurements for the band gaps identification

An analysis of the bandgaps by UV-Vis diffuse reflectance spectroscopy was executed as it is exposed in Figure 8.
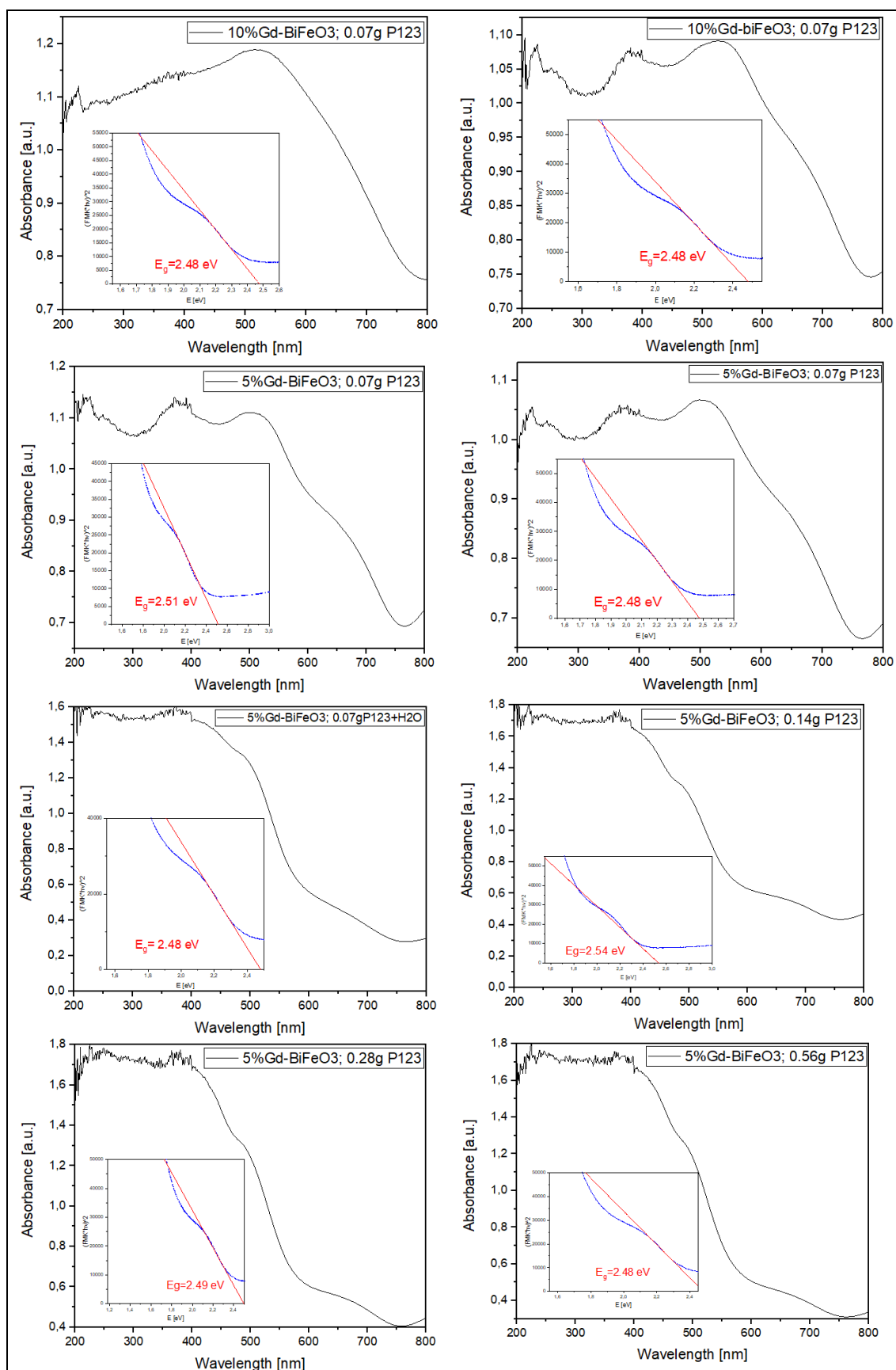
Figure 8. UV-Vis diffuse reflectance spectra from $Gd_xBi_{1-x}FeO_3$ (x=0.05, 0.10, 0.15) synthesized nanomaterials and determination its bandgaps

Accordding to the summary Table 11, it was found that the values are between 2.48-2.54 eV. This implies that neither the concentration of P123 nor the doping with gadolinium has a direct effect on the band gap.

Table 11. Band gaps of $Gd_xBi_{1-x}FeO_3$ (x=0.05, 0.10, 0.15) synthesized by the sol-gel technique

ID	Sample	P123 (g)	Bandgap (eV)	Wavelength (nm)
D1 & D3	10%-Gd BiFeO$_3$		2.48	499.93626
X		0.07	2.51	493.96093
L			2.48	499.93626
K	5%-Gd BiFeO$_3$	0.07 (+ 5ml H$_2$O)		
G		0.14	2.54	488.12674
H		0.28	2.49	497.92849
I		0.56	2.48	499.93626

3.2.3. FTIR measurements for the identification of functional groups

The FT IR measurements were executed as it is exposed in Figure 9. However, due to the low resolution, it was not possible to emit determinant conclusions about it.
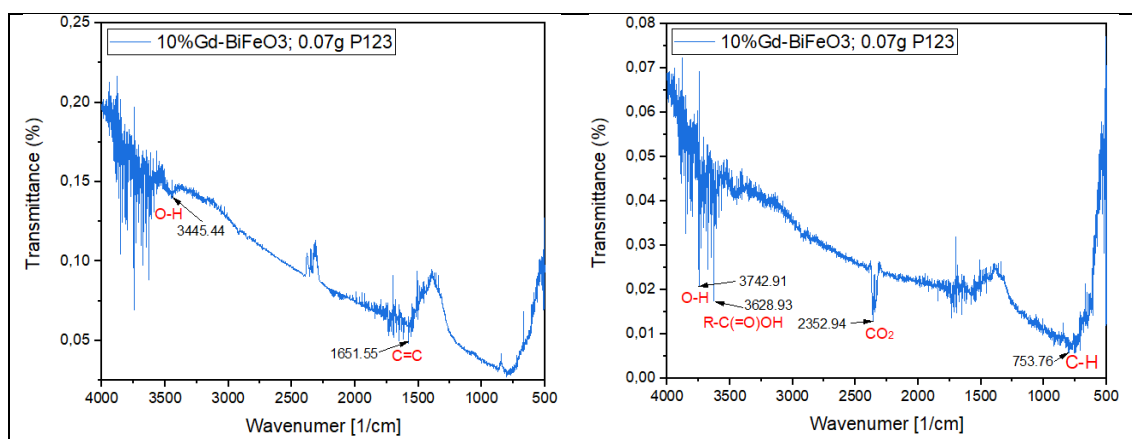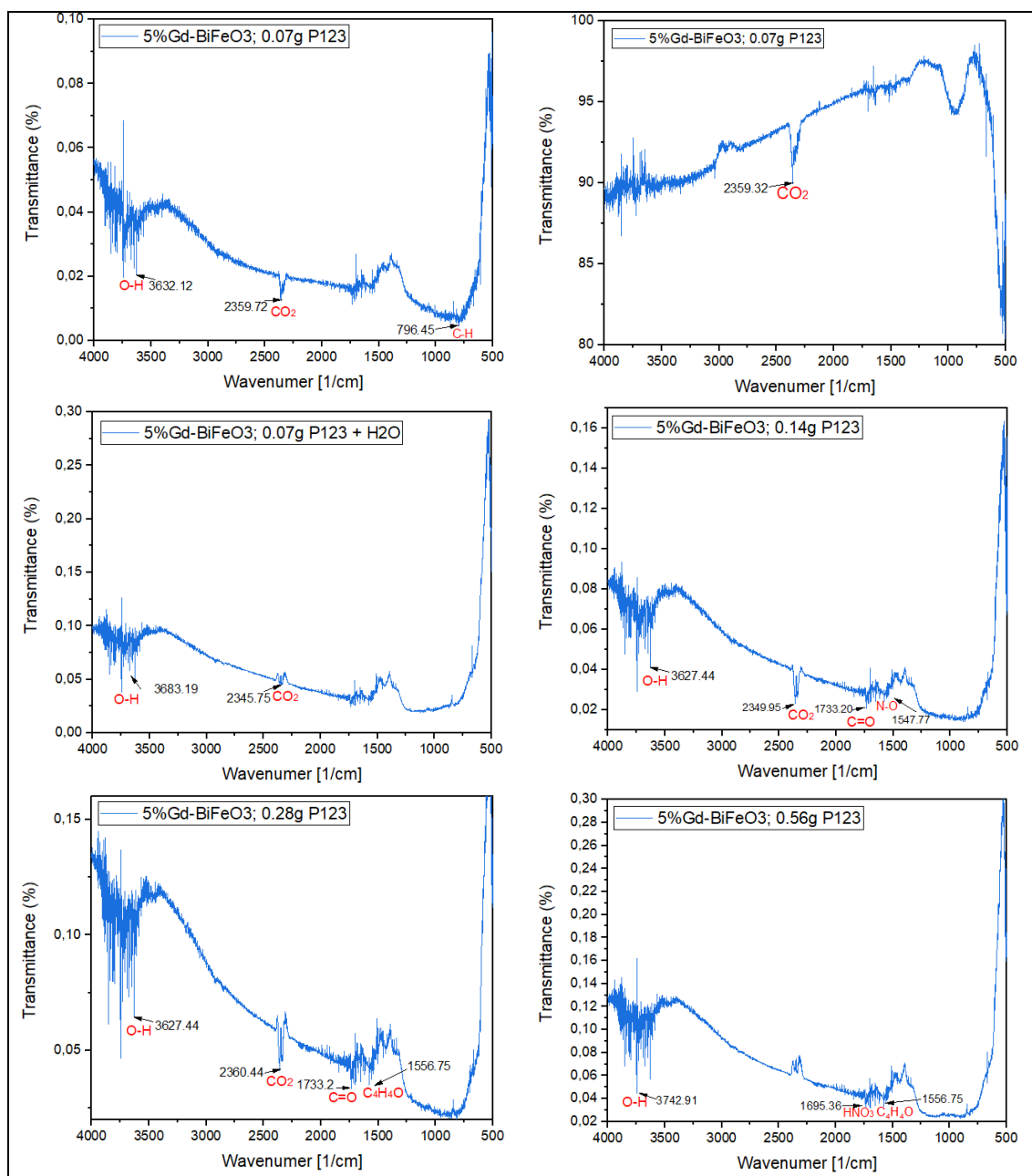
Figure 9. FT IR measurements of transmissibility from $Gd_xBi_{1-x}FeO_3$ (x=0.05, 0.10, 0.15) synthesized nanomaterials and functional groups identified

3.3. Characterization of mesoporous $Gd_xBi_{1-x}FeO_3$ (x=0.05, 0.10, 0.15) synthesized by hard templating techniques

3.3.1. Characterization of nanomaterials obtained by the two-step impregnation technique

3.3.1.1. XRD measurements for the structure analysis

The XRD of the samples presented in Figure 10 indicates that there is no significant difference between them, and unfortunately, they mostly exhibit the formation of Bi_2O_3 instead of $BiFeO_3$, which is attributable to the inadequate calcination at the end of the process. This affirmation is done considering that the final calcination of 500°C for 1h was executed separately from the heating process.
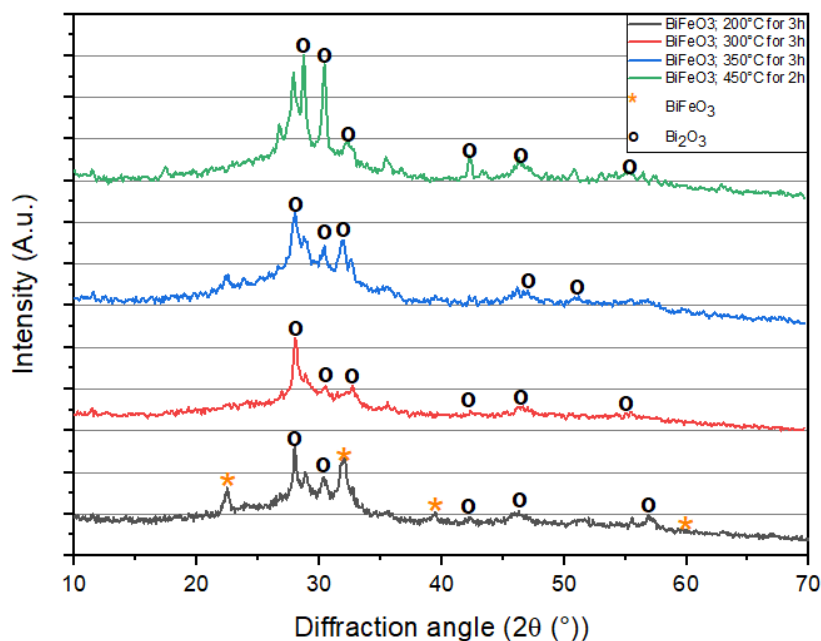
Figure 10. XRD of $BiFeO_3$ synthesized by a two-step impregnation technique

Therefore, to synthesize the nanomaterials by this method, it is required to do the calcination of 500°C for 1 hour without interruptions at the end of its correspondent calcination path.

3.3.2. Characterization of nanomaterials obtained by combustion techniques

3.3.2.1. XRD measurements for the structure analysis of samples obtained by experiment 1

Based on the XRD presented in Figure 11, it is clear that the synthesized materials exhibit an orthorhombic structure between 31-33° in the diffraction angle 2θ. Despite this, both present an excess of bismuth leading to the formation of Bi_2O_3, especially in the diffraction angle 2θ from 23-31°, which is diminishing its purity. This may be attributed to the absence of equimolar proportions of the precursors used in the process, which in composition came hydrated, in comparison to the ones used by Ghosh and collaborators (2005) during its synthesis. However, it is important to consider that due to air moisture the precursor bismuth nitrate by itself can form Bi_2O_3, which may lead to the presence of Bi_2O_3 on the final material.
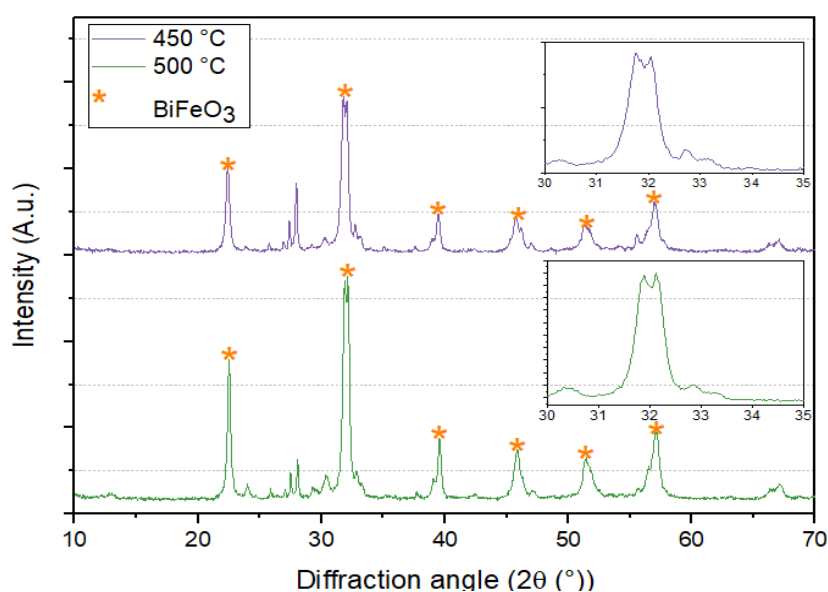
Figure 11. XRD of $BiFeO_3$ synthesized by the first experiment of a combustion technique

3.3.2.2. XRD measurements for the structure analysis of samples obtained by experiment 2

During the sample synthesis, stoichiometric equimolar proportions of the precursors were used, however, the XRD measurements of Figure 12 exhibit that the desired $BiFeO_3$ was formed partially.
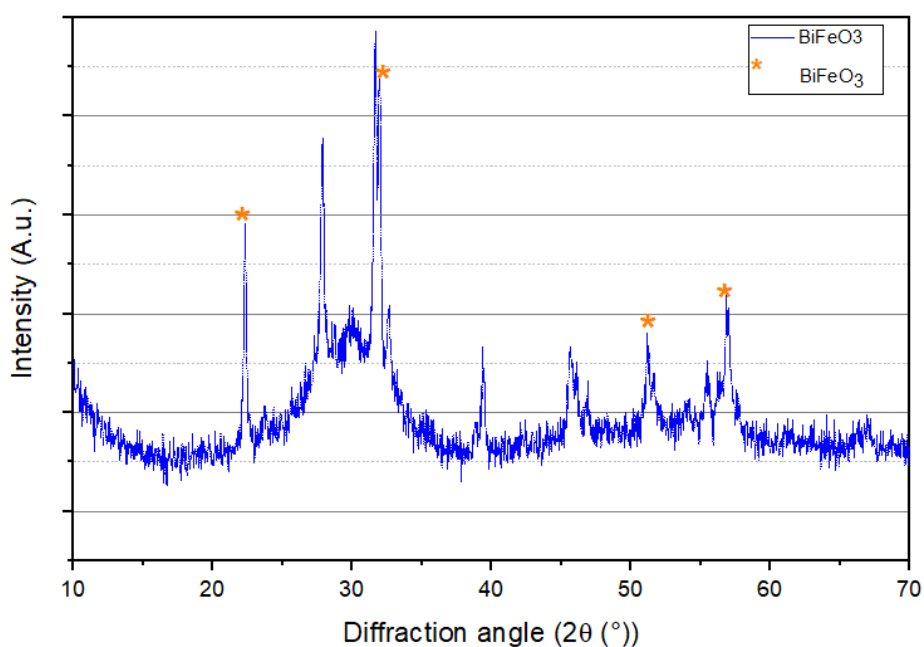
Figure 12. XRD of $BiFeO_3$ synthesized by the second experiment of a combustion technique

Therefore, the synthesis didn't work well as it was expected, because, by a similar procedure, Papadas et al. (2012) reported the formation of a 3D mesoporous network of $BiFeO_3$ nanoparticles, where 3-APA was used for the surface modification of $BiFeO_3$.

3.3.3. Characterization of nanomaterials obtained by complexation techniques

3.3.3.1. XRD measurements for the structure analysis of samples obtained by

experiment 1

The obtained sample, which structure is presented by Figure 13, was obtained having in mind the procedure of Papadas et al. (2014), in which a high surface area mesoporous BiFeO3 was synthesized, building it inside the mesoporous carbon CMK-3 (hard template).

However, the XRD didn't exhibit the formation of $BiFeO_3$ and only the formation of Bi_2O_3 was observed.
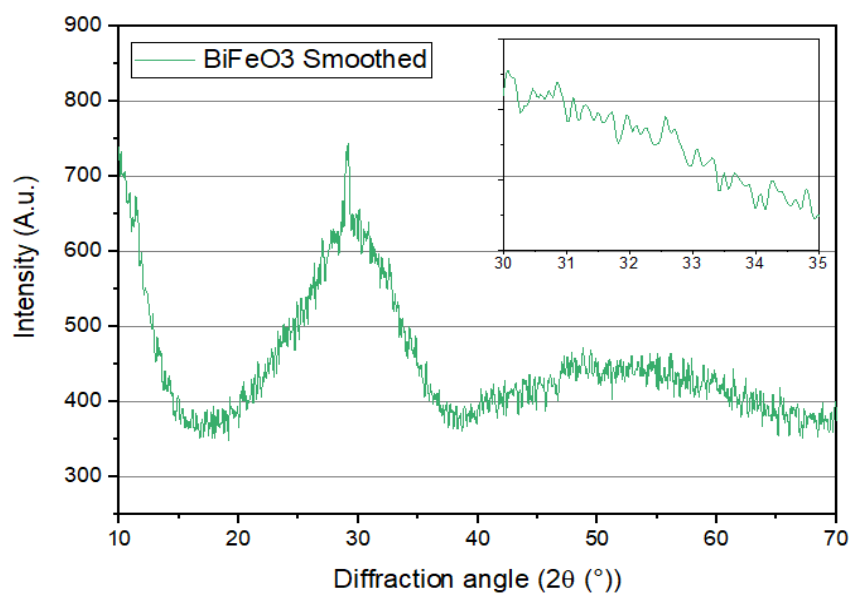
Figure 13. XRD of $BiFeO_3$ synthesized by the first experiment of a complexation

technique

3.3.3.2. XRD measurements for the structure analysis of samples obtained by

experiment 2

Considering the synthesis of $BiFeO_3$ by nano-casting developed by Lucia Morales (2019), the aim of this experiment was to enhance the photocatalytic activity of this semiconductor by doping it with 5% and 10% of Gd.

It was discovered that samples with and without bismuth excess do not display differences, as both exhibits a similar peak between 31-33° of diffraction angle 2θ, which corresponds to a typical rhombohedral structure (see figure 14). Likewise, in all of them, Bi_2O_3 is presence as shown in the peaks between 27-29°. One possible explanation is that the precursor $Bi(NO_3)_3(H_2O)_5$ contains partially Bi_2O_3 leading to stoichiometric errors in the reaction, however, XRD of the compound is required to affirm this.
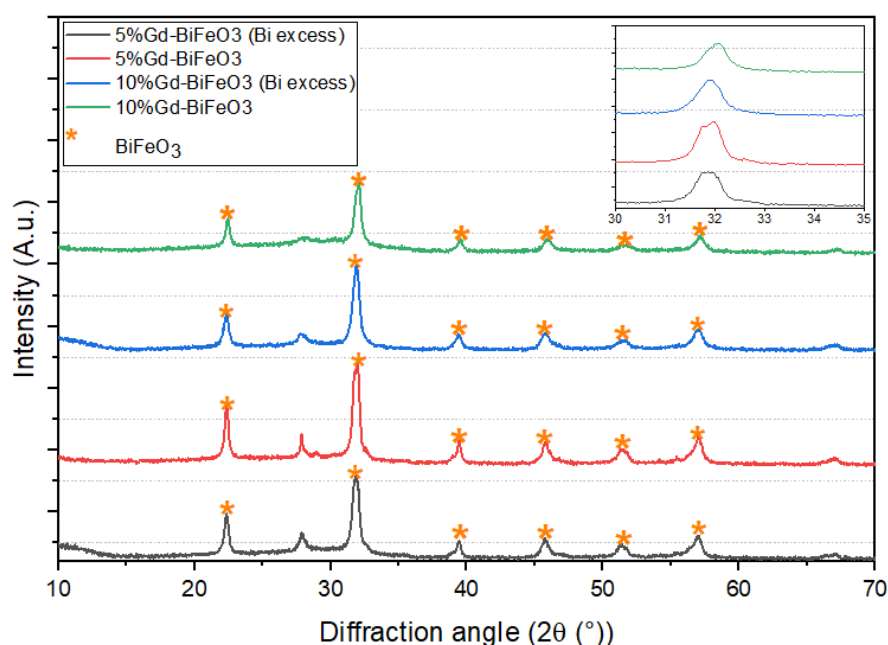
Figure 14. XRD of $Gd_xBi_{1-x}FeO_3$ (x=0.05, 0.10) synthesized by the second experiment of a complexation technique

Leaching processes were carried out for the removal of Bi_2O_3. By Figure 15, it was seen that glacial acetic acid can achieve this purpose if it is in contact with the material long

enough (10 min). Nitric acid also works but it reacts and creates unwanted phases, seen by the additional peaks 24.73° and 26.51° of the diffraction angle 2θ.
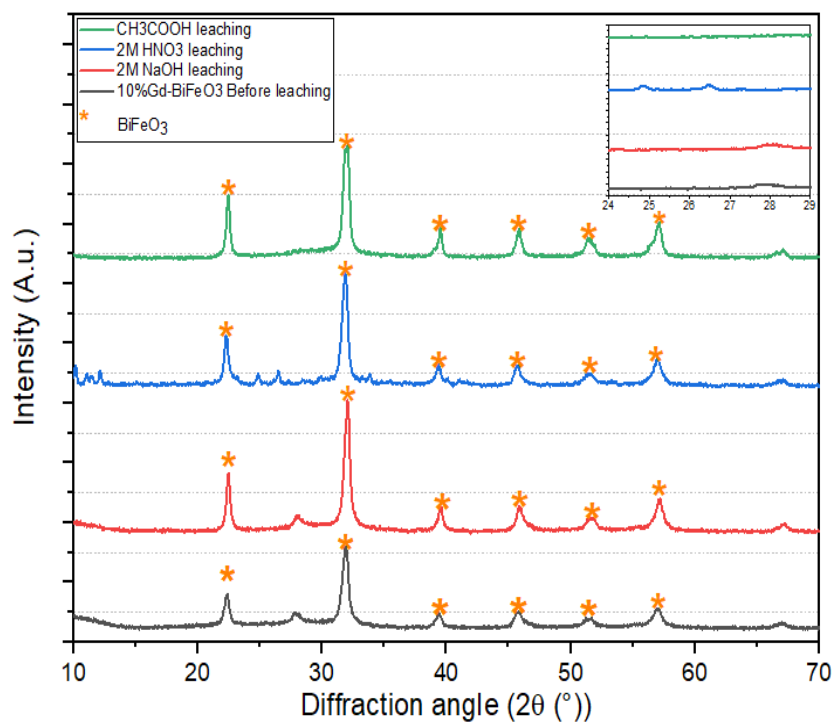
Figure 15. XRD of leached $Gd_{0.10}Bi_{0.9}FeO_3$ synthesized by the second experiment of a complexation technique

Additionally, by Figure 16 it was demonstrated that the use of half of the solvents during the synthesis didn't show a negative impact on the rhombohedral structure of the material. This constitutes a positive finding considering that 2-methoxyethanol, apart from being expensive and difficult to obtain, via inhalation and dermal contact produces effects on respiratory, nervous, reproductive and haematological systems (WHO, 2009).
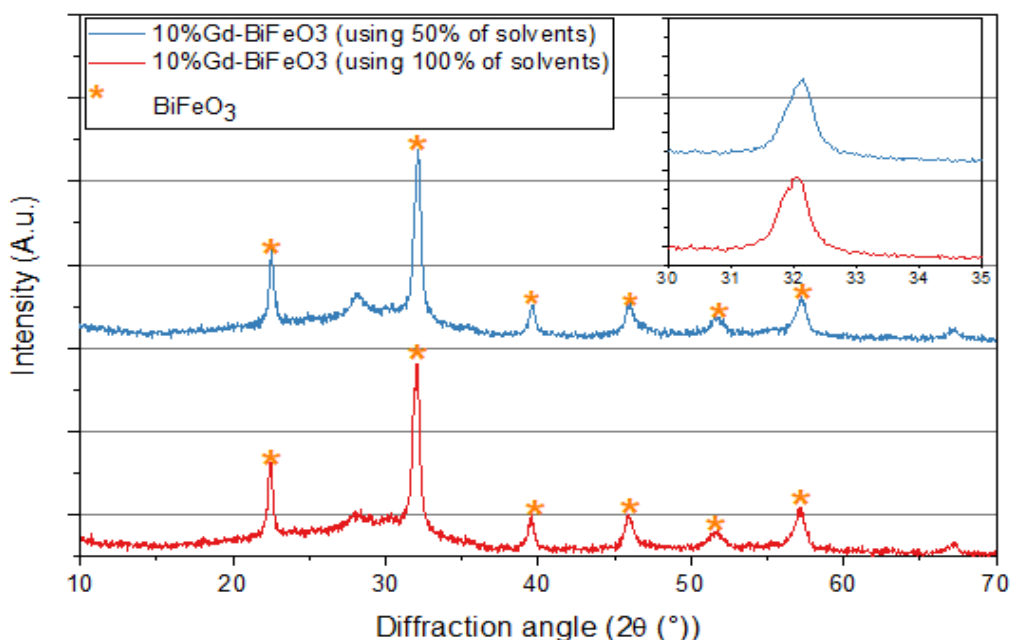
Figure 16. XRD of $Gd_{0.10}Bi_{0.9}FeO_3$ synthesized using full and half of the solvents

However, it must be considered that 2-methoxyethanol is needed during the synthesis, as it is responsible for making the bismuth-iron complex, due to the oxygen-free electrons of methoxy (OCH_3) and ethanol (CH_3CH_2OH) of the molecule that binds to the metals. Despite this, if there is too much of it, during the calcination process, it will lead to the formation of Bi_2O_3 which is seen at $2\theta = 27\text{-}29°$ of the synthesized material that use the whole amount of the solvents.

3.3.4. Characterization of nanomaterials obtained by a one-step impregnation technique

3.3.4.1. XRD measurements for the structure analysis of samples obtained by experiment 1

The XRD from Figure 17 shows that the synthesis of $BiFeO_3$ in absence of TA didn't work. This was expected considering previous XRD experiments of Papadas and collaborators (2014), where it was found that TA has a pronounced effect on the crystallization of mesoporous infiltrates as it helps to obtain a highly crystalline $BiFeO_3$

mesostructure at 1:1 molar ratio with respect to metal nitrates, promoting the crystallization of the compound inside the template.
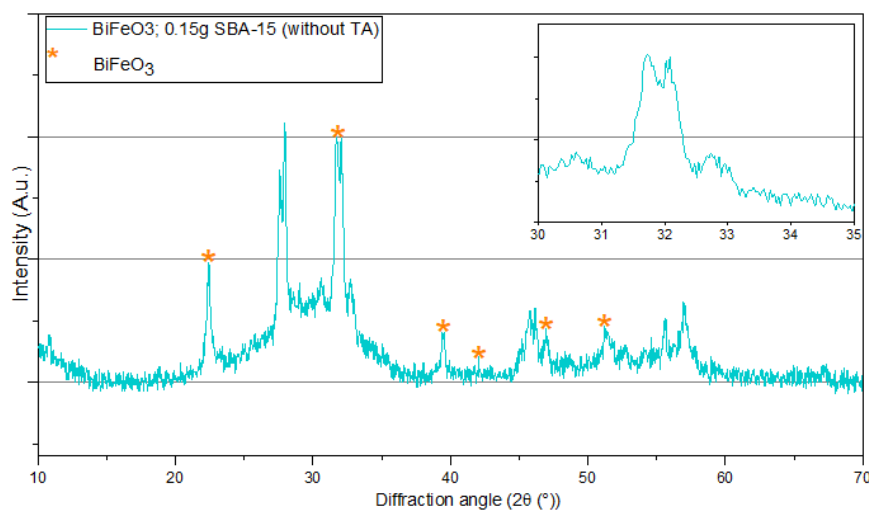
Figure 17. XRD of BiFeO$_3$ synthesized with 0.15g of SBA-15 but without TA

Despite Dang et al. (2014) find that an increase on the amounts of SBA-15 could modify the ordered mesoporous structure of Bi$_2$WO$_6$, by the resulting XRD exposed in Figure 18, it is established that the variation of the SBA-15 from 0.075g to 0.3g didn´t have a deep impact on the synthesized compounds, except on the compound that was synthesized using 0.075g of SBA-15, which exhibits a distorted rhombohedral structure of BiFeO$_3$ in the peak from 31-33° of diffraction angle 2θ. However, by the XRD of the leached compounds (plot lines: red, green and brown), it was seen that they still exhibit the peak from 26-30° of diffraction angle 2θ, which corresponds to Bi$_2$O$_3$, implying that the NaOH was not useful for its removal.
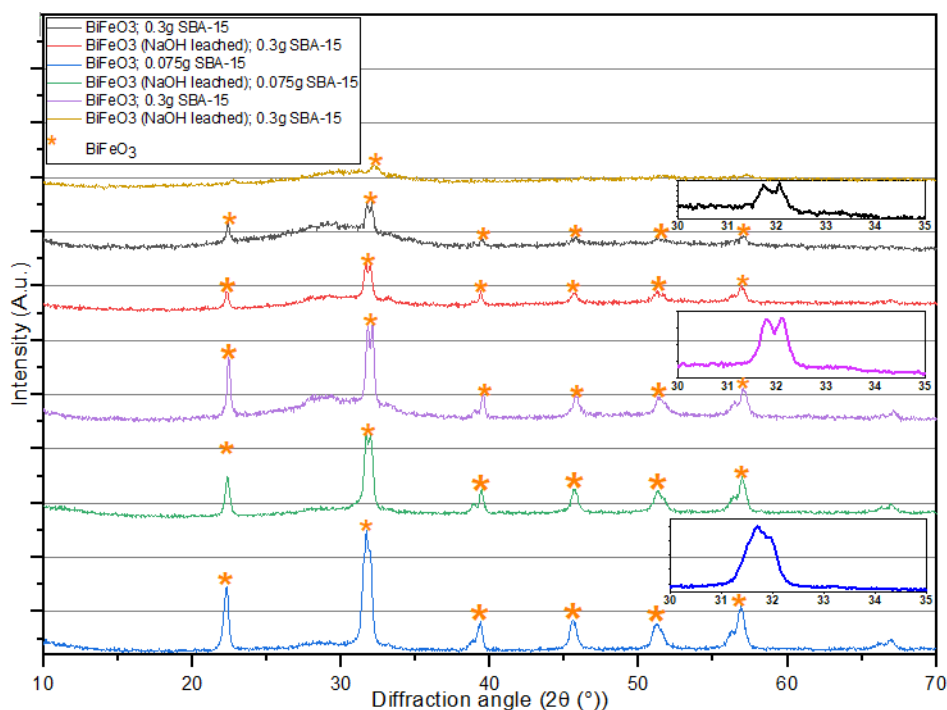
Figure 18. XRD of BiFeO$_3$ synthesized varying 0.075- 0.3g of SBA-15

By Figure 19, it is clear that similarly to BiFeO$_3$, 5%Gd- BiFeO$_3$ synthesized with 0.075g and 0.3g of SBA-15, as well as, 10%Gd- BiFeO$_3$ synthesized with 0.15g of SBA-15 conserve the rhombohedral structure in the peak from 31-33° of diffraction angle 2θ, and therefore, SBA-15 didn't affect the purity of the compounds.

However, in the case of 10%Gd- BiFeO$_3$ synthesized with 1.5g of SBA-15, the whole peaks of the diffraction angle 2θ looks unclear and from 31-33° of diffraction angle 2θ, it seems like the formation of the orthorhombic structure, which is characteristic on doped BiFeO$_3$. Therefore, by this technique, it was discovered that quantities of SBA-15 that vary from 0.075g to 0.3g have no impact on the purity of the compound and the impregnation works well. However, once the 0.3g SBA-15 are quintuplicated (1.5g), the concentration of doped BiFeO$_3$ in the XRD sample is too low in order to obtain a clear XRD pattern. It should be noted that the main peak at 32° is visible underneath the SBA15 peak.
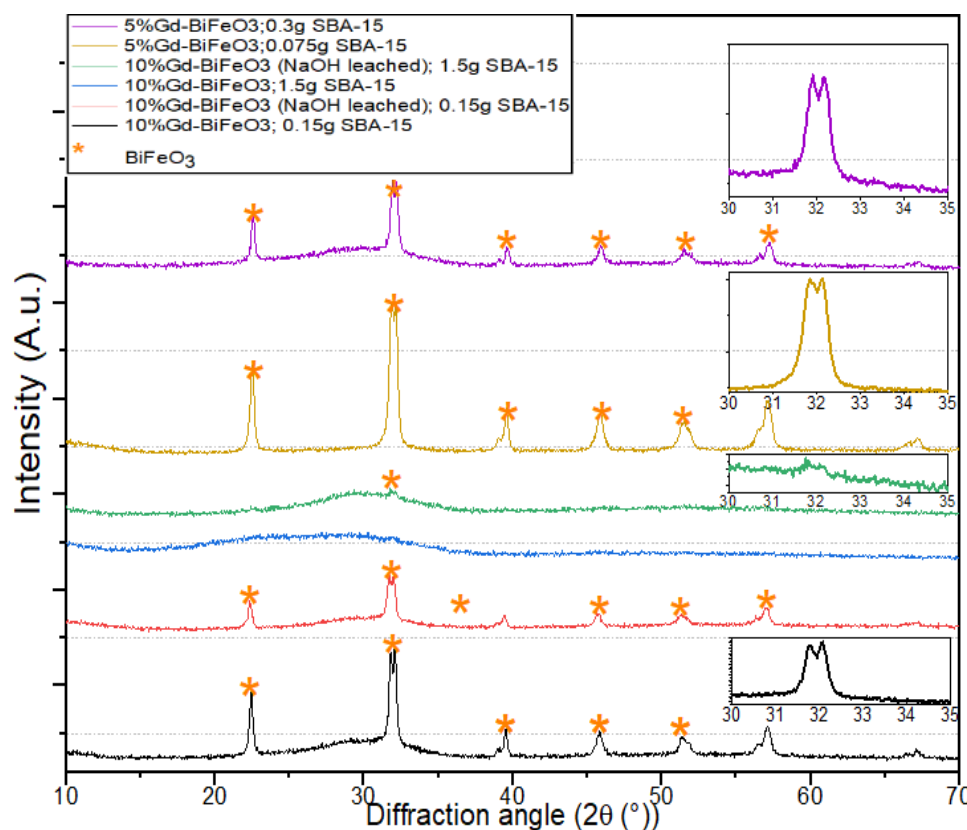
Figure 19. XRD of $Gd_xBi_{1-x}FeO_3$ (x=0.05, 0.10) synthesized using 0.075,0.15,0.3 and

1.5g of SBA-15

Finally, following the methodology of this experiment but using the stoichiometric amounts of the precursors and SBA-15 from the experiment 2, it was found that the leached synthesized powders of $BiFeO_3$ and 5%Gd- $BiFeO_3$ present an expected distorted rhombohedral structure in the peak from 31-33° of diffraction angle 2θ; which is attributed to Gadolinium substitution (see figure 20). Likewise, from 25-35° of diffraction angle 2θ, the broad peaks imply that the materials are containing an amorphous part suggesting a replica mesostructured of SBA15.
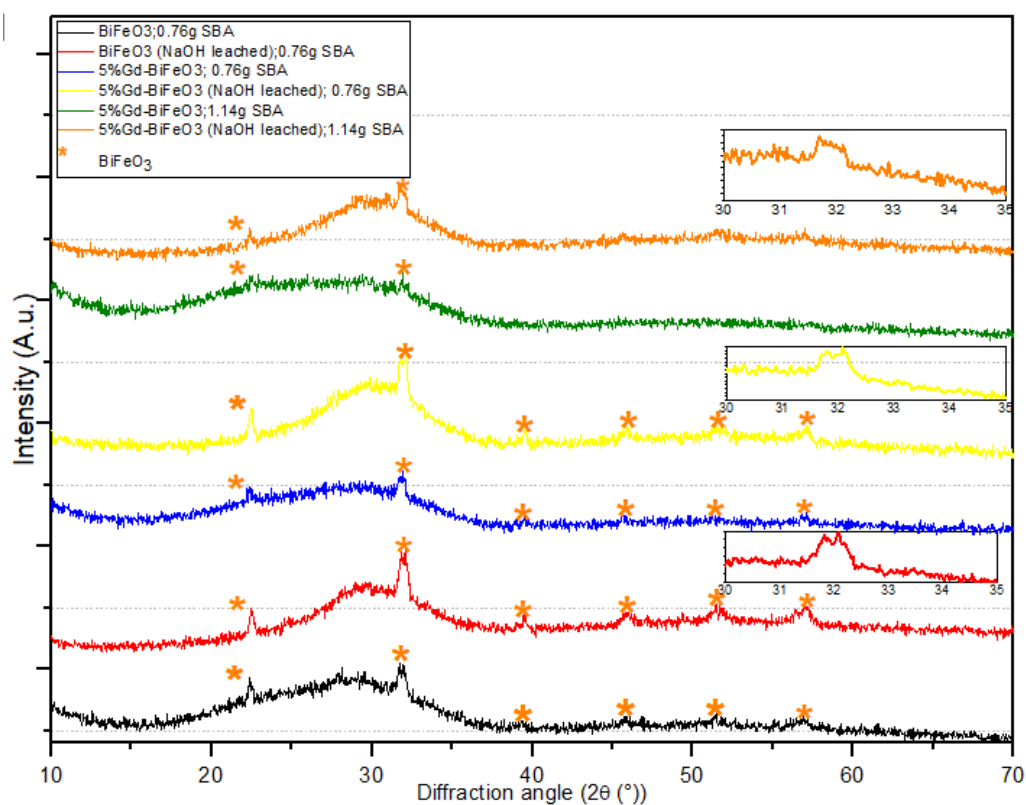
Figure 20. XRD of $BiFeO_3$ and $Gd_{0.05}Bi_{0.95}FeO_3$ synthesized using stoichiometric amounts of the precursors and SBA-15 from experiment 2 of the complexation technique

3.3.4.2. TEM measurements for the morphology analysis of samples obtained by experiment 1

Previously, by XRD results it was thought that maybe it was occurring a possible reaction between the complexes and the silica. However, considering the TEM image of Figure 21, it is clear that the silica and the $BiFeO_3$ are not reacting and they are present on the sample, but due to the agglomeration of $BiFeO_3$ in the top of the silica, it stays on the borders impeding the entrance of more $BiFeO_3$.

In the same way, the TEM measurements allow to establish that particle size of 10% Gd-$BiFeO_3$ (without NaOH leaching) was around 8nm, which is positive considering that when the size of the catalysts is smaller, more atoms accumulate in the surface, which

leads to an increase in the surface to volume ratio (Saravanan et al., 2017), and therefore, increases photocatalytic activity. In the same way, this result calls the attention once it is considered that Bi_2WO_6 synthesized with 0.3g of SBA-15 presented a particle size of 100-200 nm, leading to low particle surface area (Dang et al, 2014).
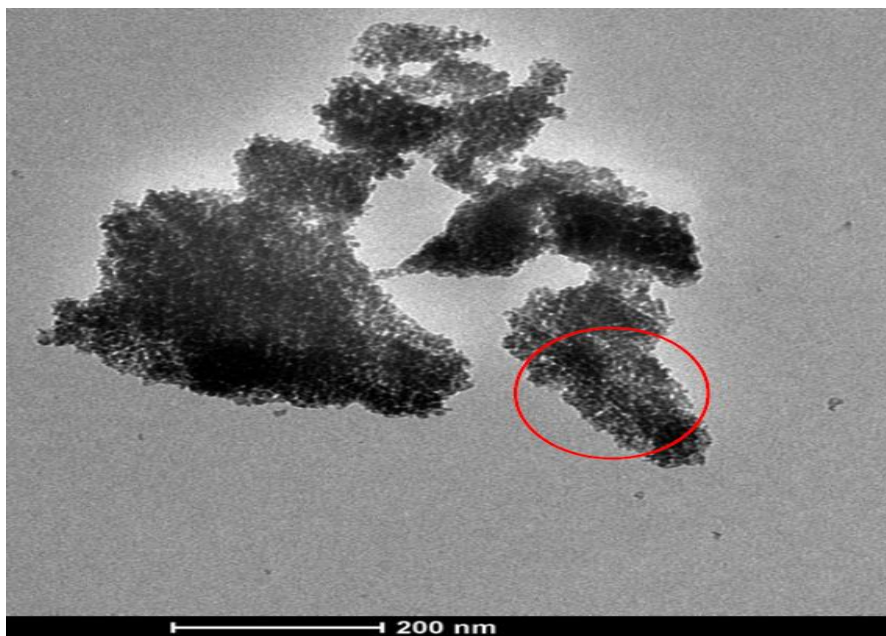
Figure 21. TEM image of $Gd_{0.10}Bi_{0.9}FeO_3$ synthesized using 1.5g SBA-15, following the developed experiment 1 of the one-step impregnation technique

3.3.4.3. XRD measurements for the structure analysis of samples obtained by experiment 2

The methodology of this experiment was developed considering that in Yen et al. (2011) it was synthesized crystalline mesoporous bimetal oxides ($NiFe_2O_4$, $CuFe_2O_4$, and Cu/CeO_2) using mesoporous silicas, in which it was applied reflux condensation of nitrate salts with hexane to obtain high surface area metal oxides. Due to this, to determine if there is a reaction between SBA-15 and the complexes, variations on the SBA-15 ratios were done.

In theory, it was expected to have more possible sites to make the reaction if there is more SBA-15, and that it should get worst if there is a reaction. However, the results exposed by Figure 22 show that with less SBA-15, it gets worst, which means that the impregnation didn´t work due to the excess material that is deposited on the top of SBA-15. Regarding this, the presence of amorphous SBA-15 broad peaks from 15-30° of diffraction angle 2θ, indicates that calcination works better in the SBA-15 channel, implying that SBA-15 has a stabilizing effect. However, in a future analysis, it would be interesting to see if after leaching with NaOH the broad peaks remain, and if this happens, this will imply that in fact, the obtained nanomaterials have an amorphous structure.
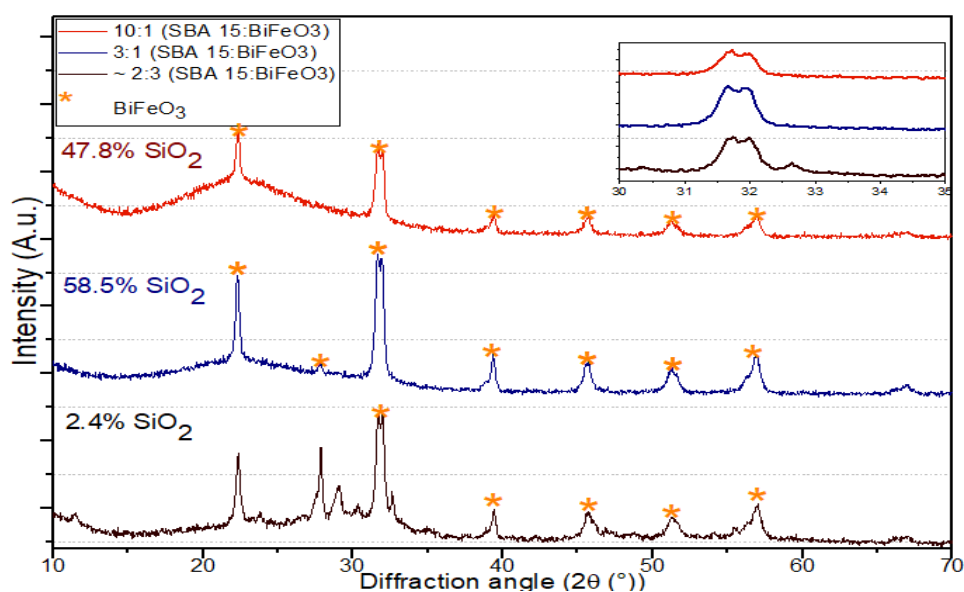
Figure 22. XRD of BiFeO$_3$ synthesized using different ratios of SBA-15: BiFeO3

3.3.4.4. TEM measurements for the morphology analysis of samples obtained by experiment 2

Considering the TEM images presented in Figure 23, it is noteworthy that nanoparticles of BiFeO$_3$ with a diameter of approximately 24nm were obtained after leaching with NaOH the synthesized sample using BiFeO$_3$ a ratio of 2 parts of SBA-15 per 3 parts of BiFeO$_3$.
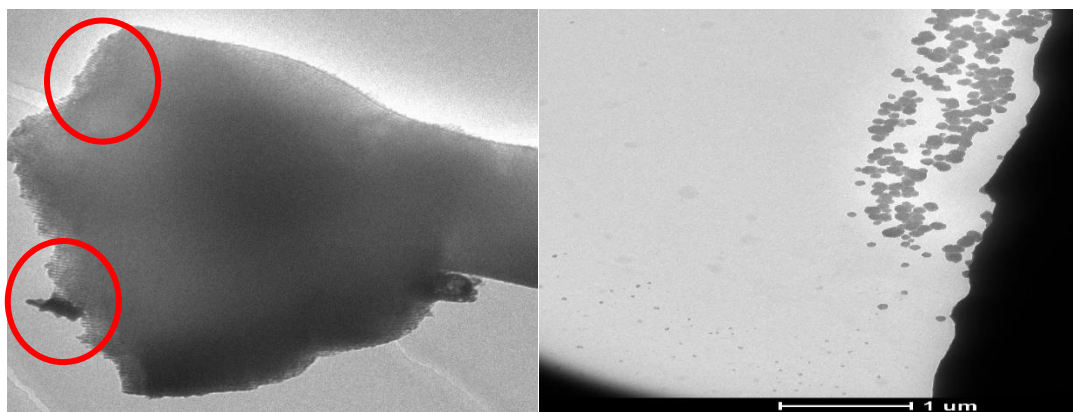
Figure 23. TEM images of the synthesized BiFeO$_3$ with a ratio of 2 SBA-15: 3 BiFeO$_3$, before (left) and after (right) leaching with NaOH

Additionally, in order to see the dependence of the nano-casted structures with the precursor and silica loadings, TEM measurements of BiFeO$_3$ synthesized with 10 parts of SBA-15 per 1 part of BiFeO$_3$ were done. By Figure 24, it is clear the formation of particles with an approximate size of 8nm. This suggests that an increase in the amount of SBA-15 leads to the formation of small particles, which goes according to the observations of Yen and collaborators (2011), in which it passes from nanorods to nanowires once the precursors were increased per amount of silica.
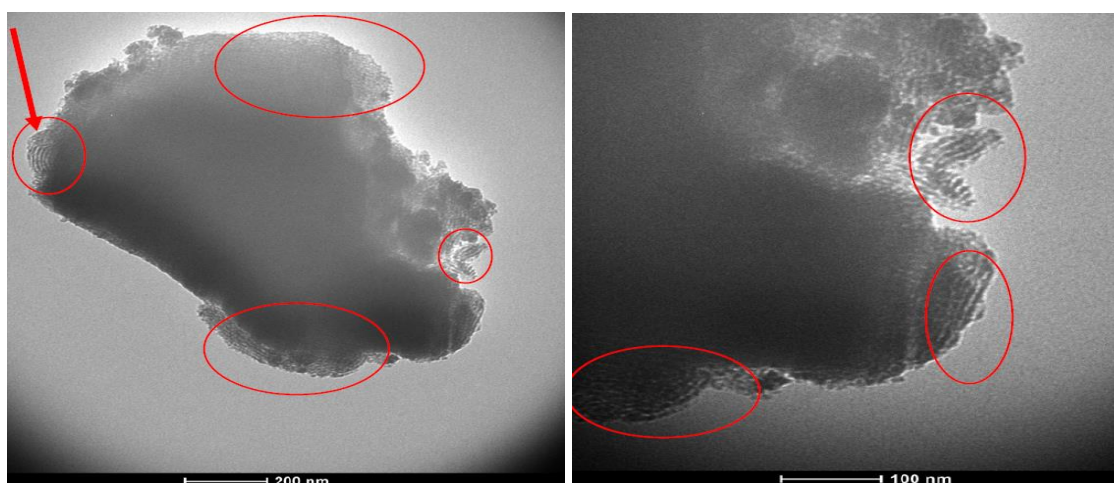
Figure 24. TEM images of the synthesized BiFeO$_3$ with a ratio of 10 SBA-15: 1 BiFeO$_3$ before leaching with NaOH

3.4. Photocatalytic activity

Following the photocatalytic procedure described in the section of the experimental description, the measurements allow the obtention of the following calculations and plots for the analysis of the photocatalytic degradations of RhB.

3.4.1. Detailed analysis of the RhB degradation

3.4.1.1. $Gd_xBi_{1-x}FeO_3$ (x=0.05, 0.10, 0.15) synthesized by a soft templating technique

Considering the plots from Figure 25 of 5%Gd-BiFeO$_3$ synthesized using 0-07-0.28g of P123, it is clear that the slight increase on degradation degree and rate when little amount of P123 was used can be neglected and therefore it can be affirmed that in overall the samples achieved 41-59% of RhB degradation at a rate of 2.54 - 4,46E-03 min^{-1}.
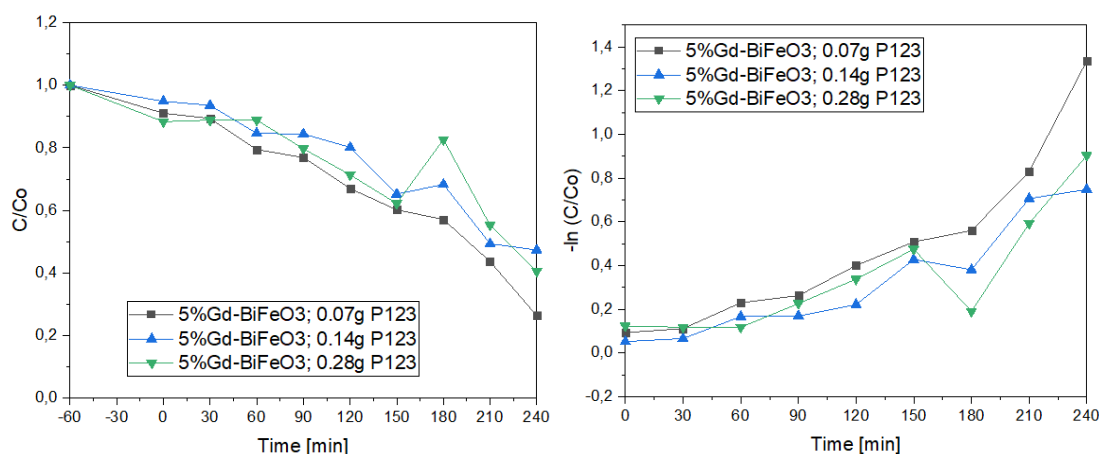
Figure 25. Photocatalytic activity of $Gd_{0.05}Bi_{0.95}FeO_3$ synthesized using 0-07-0.28g of P123

Additionally, by Figure 26, it is clear that using the same 0.07g of P123 for the synthesis of the samples, the doping amount influences the degree and rate of degradation, in which 5%Gd-BiFeO$_3$ performed the higher 73% of degradation at 4,46E-03 min^{-1}.

This last result calls the attention when it is compared with 57% degradation of Methyl Orange in 3h reported by Song and collaborators (2009), essentially due to the difficulty of degradation that RhB poses, as it is positively charged in H_2O having a repulsive interaction when it is in contact with the positive charges of the metals (Fe^{3+}, Bi^{3+} and/or Gd^{3+}); while Methyl Orange is attracted to the semiconductor particle surface as it is a negatively charged dye in H_2O.
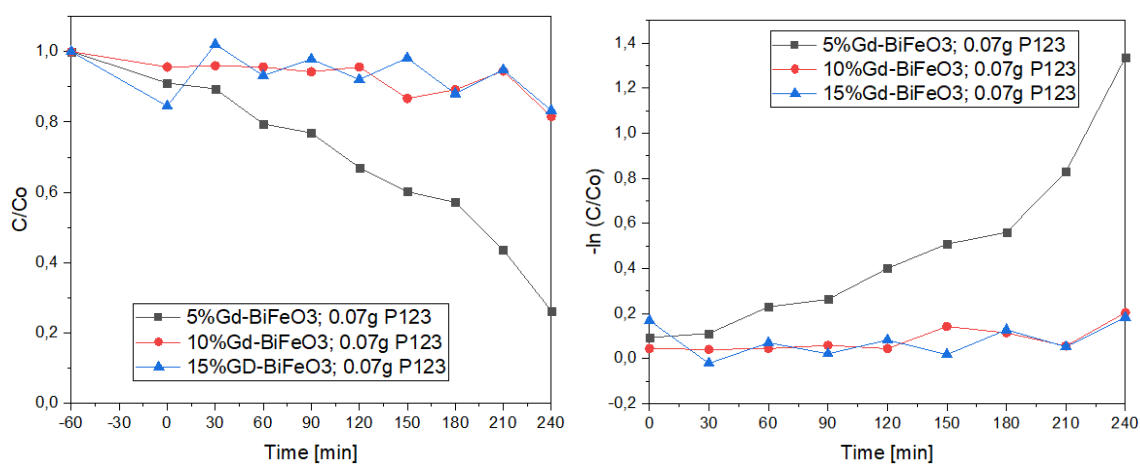
Figure 26. Photocatalytic activity of $Gd_xBi_{1-x}FeO_3$ (x=0.05, 0.10, 0.15) synthesized using 0-07g of P123

3.4.1.2. $Gd_xBi_{1-x}FeO_3$ (x=0.05, 0.10) synthesized by the experiment 2 of the complexation technique

Considering the plots of Figure 27, it is clear an efficient RhB degradation achieved by the 5% and 10% Gd- $BiFeO_3$ before NaOH leaching, in which the rate and degree of degradation of RhB are slightly higher in the sample of 10%Gd- $BiFeO_3$ synthesized using half of the solvents. However, once the 5%Gd-$BiFeO_3$ sample was leached with NaOH, the degree of degradation decrease, which suggests that SBA-15 is contributing to the removal of RhB from the sample.

This result goes according to the findings of Srinivasan and collaborators (2015), whereby using SnO_2 nanoparticles embedded in SBA-15, it was maximized the photocatalytic activity during the degradation of RhB; which is attributed to the shorter diffusion path-length of RhB molecules inside SBA-15.
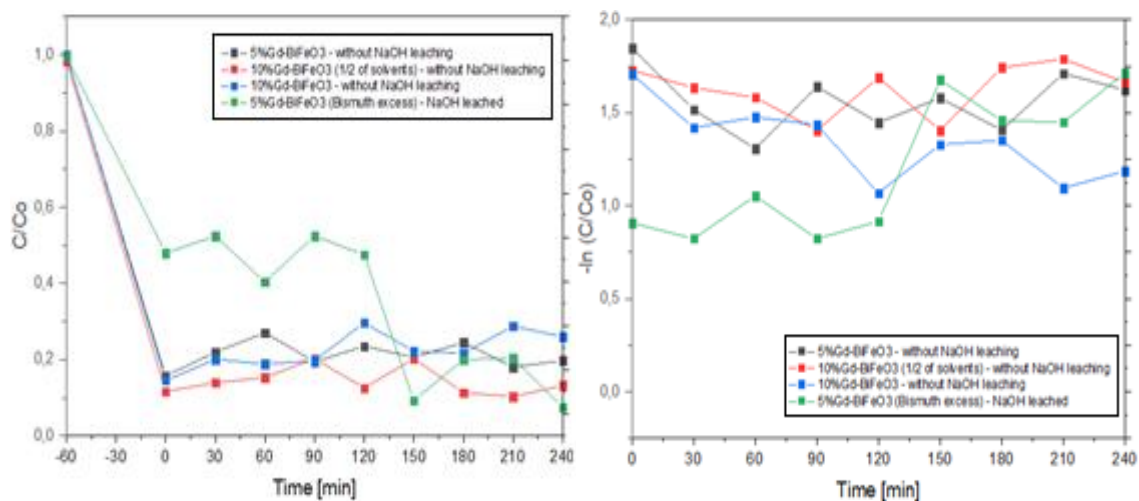
Figure 27. Photocatalytic activity of $Gd_xBi_{1-x}FeO_3$ (x=0.05, 0.10) synthesized by the second experiment of a complexation technique

3.4.1.3. $BiFeO_3$ and $Gd_xBi_{1-x}FeO_3$ (x=0.05, 0.10, 0.15) synthesized by the experiment 1 of the one-step impregnation technique

According to the plots presented by Figure 28, it is clear that RhB degradation starts during darkness, since the first moment that the dye was in contact with the catalyst. This suggests that due to the small size of the particles, efficiently ·OH radicals are produced and degrade the dye. However, it calls the attention that there is an imperceptible difference in degradation between samples synthesized with 0.075, 0.15 or 1.5g of SBA-15, implying that SBA-15 does not influence the degree or rate of degradation performed by 5% and 10%Gd-$BiFeO_3$ samples.
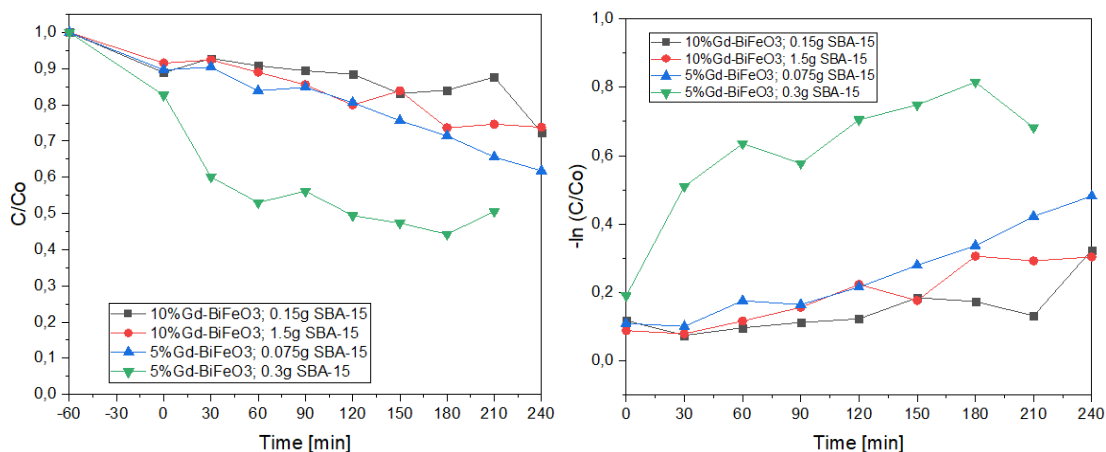
Figure 28. Photocatalytic activity of $Gd_xBi_{1-x}FeO_3$ (x=0.05, 0.10) synthesized by the first experiment of the one-step impregnation technique

Regarding the analyzed samples, 5%Gd-BiFeO$_3$ synthesized using 0.3g of SBA-15 have a greater 49% degradation achieved at 2,16E-03 min^{-1}, which suggests by the one-step impregnation technique, doping of Gd with 5% and using 0.3g of SBA-15 is ideal.

Additionally, as it is presented in Figure 29, BiFeO$_3$ samples synthesized by this technique exhibit similar 19-34% of degradation that is independent of the 0.075-0.3g of SBA-15; confirming that the variation does not influence the photocatalytic activity.
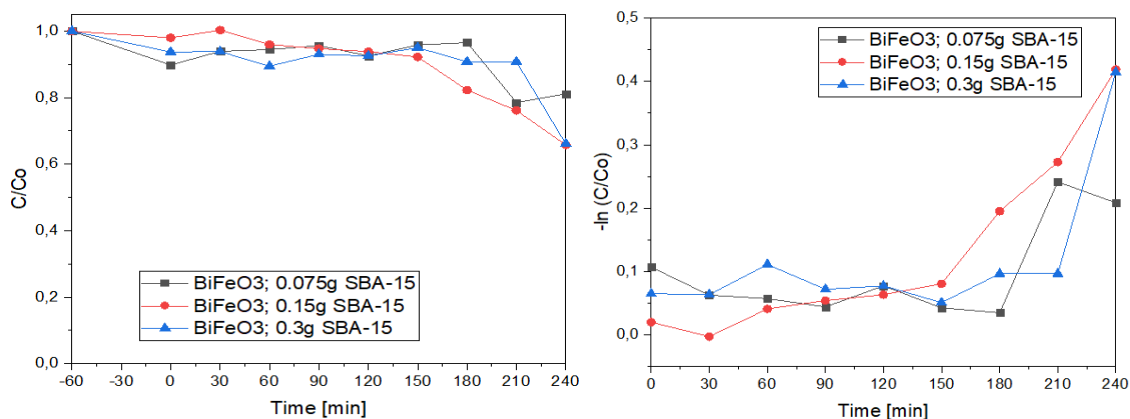
Figure 29. Photocatalytic activity of BiFeO$_3$ synthesized varying the SBA-15 from 0.075-0.3g

3.4.1.4. BiFeO$_3$ synthesized by experiment 2 of the one-step impregnation technique

Considering Figure 30, it is clear that the variation of the ratios between SBA-15 and BiFeO$_3$ does not have a negative impact on the degree of degradation, as 10 SBA-15: 1 BiFeO$_3$ and 3 SBA-15: 1 BiFeO$_3$ achieved an average 80% degradation at a rate of 1.4E-03 min^{-1}.
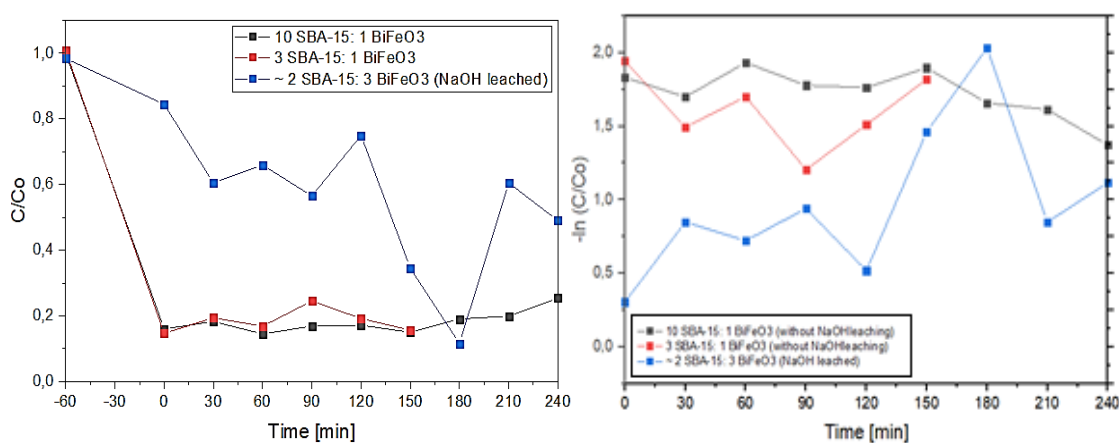
Figure 30. Photocatalytic activity of BiFeO$_3$ synthesized using different ratios of SBA-15 and BiFeO$_3$

Similar to previously described samples that were synthesized by the complexation technique, these samples also display a high removal of RhB since the first moment that the catalyst was in contact with the dye.

Specifically, in order to know if there is degradation and not only absorption, from the final material SBA-15 can be released and in that way, it will be identified how much of the synthesized material is on it; but it is difficult without decomposing. However, only considering the current results, apart from the fact that SBA-15 can absorb RhB much better because it is negatively charged in comparison with RhB that is positively charged; it must be considered that BiFeO$_3$ has a porous surface area which theoretically also absorbs some quantity of the dye, but most likely it just degrades it.

3.4.2. Degrees and rates of RhB degradation of the overall synthesized samples

By Table 12, where it is presented the percentage and rate of degradation per synthesized samples, with or without leaching depending on the specific requirements, it is clear that samples synthesized by hard templating techniques where SBA-15 was used, degrade more quickly and in a higher degree RhB. Which as previously was described, is attributed to the presence of the complex SBA-15-catalyst, in which the dye respectively is absorbed and degraded.

However, regarding samples synthesized by the soft templating technique using P123, it was noticeable that 5%Gd-BiFeO$_3$ is the one that achieves an efficient degradation in time and amount, when it is compared with the synthesized samples doped with 10% and 15% of Gd. And as it was seen in XRD analysis, it is confirmed that the amount of P123 used during the synthesis, does not impact the catalysts, as negligible variations of the rate and degree of degradation were observed.

Table 12. Summary of the photocatalytic degradations of RhB

ID	Sample	Chemical used for leaching	k (min^{-1})	% Degradation
5L	5%Gd- BiFeO$_3$	-	2,98E-03	80%
10LA	10%Gd- BiFeO$_3$ (1/2 of solvents)	-	2,69E-03	74%
10LB	10%Gd- BiFeO$_3$	-	1,59E-03	74%
2L	5%Gd- BiFeO$_3$ (Bismuth excess)	CH$_3$COOH	5,37E-04	18%
R	10 SBA-15: 1 BiFeO$_3$	-	1,40E-03	75%
3R	3 SBA-15: 1 BiFeO$_3$	-	1,41E-03	93%
UPS	~ 2 SBA-15: 3 BiFeO$_3$	NaOH	2,84E-04	9%
A	BiFeO3; 0.075g SBA-15	NaOH	4,99E-04	19%
B	BiFeO3; 0.15g SBA-15	NaOH	1,53E-03	34%
C	BiFeO3; 0.3g SBA-15	NaOH	8,04E-04	34%
E	10%Gd- BiFeO$_3$; 0.15g SBA-15	NaOH	6,80E-04	28%

F	10%Gd- BiFeO$_3$; 1.5g SBA-15	-	1,06E-03	26%
Y	5%Gd- BiFeO$_3$; 0.075g SBA-15	-	1,61E-03	38%
Z	5%Gd- BiFeO$_3$; 0.3g SBA-15	-	2,16E-03	49%
P1	BiFeO$_3$; 0.76g SBA-15	-	8,71E-04	17%
P2	5%Gd- BiFeO$_3$; 0.76g SBA-15	-	3,24E-04	53%
P3	BiFeO$_3$; 1.14g SBA-15	-	3,84E-03	65%
D1	10%Gd- BiFeO$_3$; 0.07g P123	-	6,49E-04	21%
D1	10%Gd- BiFeO$_3$; 0.07g P123	CH$_3$COOH	1,48E-03	30%
D2	10%Gd- BiFeO$_3$; 0.07g P123	-	5,04E-04	18%
15P	15%Gd- BiFeO$_3$; 0.07g P123	-	2,17E-04	17%
G	5%Gd- BiFeO$_3$; 0.14g P123	-	2,99E-03	53%
H	5%Gd- BiFeO$_3$; 0.28g P123	-	2,74E-03	60%
X	5%Gd- BiFeO$_3$; 0.07g P123	-	4,46E-03	73%

4. Conclusions

Synthetic procedures of soft and hard templating were successfully developed that improve the formation of crystalline nanostructured BiFeO$_3$ and Gd$_x$Bi$_{1-x}$FeO$_3$ (x=0.05, 0.10, 0.15), which show enhanced photocatalytic activity for the degradation of dyes, like RhB.

The synthesized materials possess a rhombohedral structure that changes to an orthorhombic structure when doping with 5,10 and 15% of Gd. However, the purity of some of the samples was diminished by the presence of Bi$_2$O$_3$ that was intended to be removed by the leaching process with nitric acid, but it was discovered that once glacial acetic acid was in contact with the material, it efficiently can remove the undesirable bismuth oxides.

Specifically, the nanomaterials obtained from the soft templating technique, suggests that P123 is inert, as the results give the excess to highly porous $BiFeO_3$ particles or even $BiFeO_3$ hollow spheres. In addition, Gd doping does not alter the band gaps that go from 2.48-2.54 eV, but it is needed for the stabilization of the excited electrons. Finally, it was observed that 5%Gd-$BiFeO_3$ has higher photocatalytic activity, achieving a 73% of RhB degradation at 4,46E-03 min^{-1}.

Regarding the samples obtained from the hard templating techniques, it was found that SBA-15 is inert, as phase purity of $BiFeO_3$ and $Gd_xBi_{1-x}FeO_3$ (x=0.05, 0.10, 0.15) is obtained even under excess of this silica template. In addition, nanoparticles of around 8nm and 24nm were obtained, respectively by the synthesis of 10%Gd- $BiFeO_3$ (without NaOH leaching) using 1.5g of SBA-15 and $BiFeO_3$ with a ratio of 2 SBA-15: 3 $BiFeO_3$. This is positive considering that in smaller catalysts, more atoms accumulate in the surface, leading to an increase in the surface to volume ratio for the degradation of dyes.

Another discovery was about the synthesis procedures that imply the use of 2-methoxyethanol, by which no negative impact was observed on the rhombohedral structure of the material, implying that the solvent can be reduced by a half or even less. However, it must be used for the formation of Bi/Fe complexes under the presence of TA and nitric acid.

Finally, it was seen that SBA-15 and $BiFeO_3$ can form a composite material with largely enhanced photocatalytic activities for RhB degradation. SBA-15 acts like a sponge that absorbs the dye while the pure or doped $BiFeO_3$ generates ·OH that degrades the dye. Therefore, this opens the possibility of a new research project in which experiments can be done to find the best technique to synthesized composite materials that can enhance even more the photocatalysis activity for the degradation of dyes.

5. References

Aneyo, I., Doherty, F., Adebesin, O., & Hammed, M. (*2016*). Biodegradation of Pollutants in Waste Water from Pharmaceutical, Textile and Local Dye Effluent in Lagos, Nigeria. *Journal of Health and Pollution*, Vol. 6, No. 12, pp. 34-42, DOI: 10.5696/2156-9614-6.12.34

Bai, X.F., Wei, J., Tian, B.B., Liu, Y., Reiss, T., Guiblin, N., Gemeiner, P., Dkhill, B. & Infante, I.C. (2016). Size Effect on Optical and Photocatalytic Properties in $BiFeO_3$ Nanoparticles. *The Journal of Physical Chemistry*, 120 (7), pp. 3595-3601. DOI: 10.1021/acs.jpcc.5b09945

Dang, X., Dong, X., Wang, H., Zhang, X., Ma, H. & Xue, M. (2014). Controllable Fabrication of Ordered Mesoporous Bi_2WO_6 and Its High Photocatalytic Activity under Visible Light. *International Journal of Photoenergy*, V. 2014, ID. 146892. DOI: http://dx.doi.org/10.1155/2014/146892

Deng, X., Chen, K. & Tüysüz, H., (2016). A Protocol for the Nanocasting Method: Preparation of Ordered Mesoporous Metal Oxides. *Chemistry of Materials*, DOI: 10.1021/acs.chemmater.6b02645

Emy Marlina, S., Sze Nee,G., Ta Yeong, W., Tan, T., Sharifah Bee, A.H. & Joon Ching, J. (2015). Evaluation on the Photocatalytic Degradation Activity of Reactive Blue 4 using Pure Anatase Nano-TiO2. *Sains Malaysiana* 44 (7), pp.1011-1019. DOI: 10.17576/jsm-2015-4407-13

European Commission. (2000). Directive 2000/60/EC of the European Parliament and of the council of 23 rd October 2000 establishing a framework for community action

in the field of water policy. Official Journal of the European Communities, L327/1. Brussels, European Commission.

Gebreslassie, T.W., Pattabi, M. & Pattabi, R.M. (2013). Review on the Photocatalytic Degradation of Dyes and Antibacterial Activities of Pure and Doped-ZnO. *International Journal of Science and Research (IJSR)*, Volume 4 Issue 5. Paper ID: SUB167019.

Guo, R., Fang, L., Dong, W., Zheng, F., & Shen, M. (2010). Enhanced Photocatalytic Activity and Ferromagnetism in Gd Doped BiFeO3 Nanoparticles. *The Journal of Physical Chemistry C*, 114(49), 21390–21396. DOI: 10.1021/jp104660a

Gürses, J., Akın, B. & Özgür, M. (2016). Ultrasonic-assisted adsorption of methylene blue on sumac leaves. *Desalination and water treatment 57: 9286*-9295, https://DOI.org/10.1080/19443994.2015.1029002

Hassaan, M.A. & El Nemr, A. (2017). Health and Environmental Impacts of Dyes: Mini Review. *American Journal of Environmental Science and Engineering*, 1 (3), 64-67. DOI: 10.11648/j.ajese.20170103.11

Humayun, M., Zada, A., Zhijun, A., Xie, M., Xuliang, Z., Qu, Y., Raziq, F. & Jing, L. (2016). Enhanced visible-light activities of porous BiFeO 3 by coupling with nanocrystalline TiO 2 and mechanism. *Applied Catalysis B: Environmental*, 180, 219–226. DOI: 10.1016/j.apcatb.2015.06.035

Ibhadon, A., & Fitzpatrick, P. (2013). Heterogeneous Photocatalysis: Recent Advances and Applications. Catalysts, 3(1), 189–218. DOI: 10.3390/catal3010189

International Agency for Research on Cancer (IARC). (2019). Agents classified by the IARC Monographs. World Health Organization.

Jain, R., Mathur, S., Sikarwar, S. & Mittal, A. (2007). Removal of the hazardous dye rhodamine B through photo catalytic and adsorption treatments. *Journal of Environmental Management* 85, pp. 956-964, DOI: https://DOI.org/10.1016/j.jenvman.2006.11.002

Jiao, S., Zhao, Y., Li, C., Wang, B. & Qu, Y. (2018). Recyclable adsorbent of BiFeO3/Carbon for purifying industrial dye wastewater via photocatalytic reproducible. *Green Energy & Environment, 4, pp. 66-74, DOI:* https://DOI.org/10.1016/j.gee.2018.05.001

Khani, R., Sobhani, S., & Yari, T. (2019). Magnetic dispersive micro solid-phase extraction of trace rhodamine B using imino-pyridine immobilized on iron oxide as nanosorbent and optimization by Box–Behnken design. *Microchemical Journal*, 146, 471-478. DOI:10.1016/j.microc.2019.01.038

Kleitz,F., Choi, S. & Ryoo, R. (2003). Cubic Ia3d Large Mesoporous Silica: Synthesis and Replication to Platinum Nanowires, Carbon Nanorods and Carbon Nanotubes. *Chemical Communications*, pp. 2136-2137, DOI: 10.1039/B306504A

Kubelka, P. & Munk, F. (1931). A contribution to the appearance of the Paint. *Journal of Technical Physics*, 12, 593-601.

Lotey, G. S., & Verma, N. K. (2013). Gd-doped BiFeO3 nanoparticles – A novel material for highly efficient dye-sensitized solar cells. *Chemical Physics Letters*, 574, 71–77. DOI: 10.1016/j.cplett.2013.04.046

Luo, W., Zhu, L., Wang, N., Tang, H., Cao, M., & She, Y. (2010). Efficient Removal of Organic Pollutants with Magnetic Nanoscaled BiFeO3 as a Reusable Heterogeneous Fenton-Like Catalyst. Environmental Science & Technology, 44(5), pp. 1786-1791. DOI: 10.1021/es903390g

Mamun, K., Kurny, A., & Gulshan, F. (2017). Parameters affecting the photocatalytic degradation of dyes using TiO2: A Review. *Journal of Hazardous Materials*, V. 170, Issues 2-3, pp. 520-529. DOI: https://doi.org/10.1016/j.jhazmat.2009.05.039

Masi, F., Rizzo, A., Bresciani, R., Martinuzzi, Wallace, S.D., Van Oirschot, D., Macor, F., Rossini, T., Fornarolli, R. & Mezzanotte, V. (2019). Lessons learnt from a pilot study on residual dye removal by an aerated treatment wetland. *Science of the Total Environment*, 648, pp. 144-152, DOI: https://DOI.org/10.1016/j.scitotenv.2018.08.113

Morales, L. (2019). Design and application of advanced $BiFeO_3$ nano-materials for the photodegradation of organic pollutants in wastewater systems. Tesis (Ingeniería Química). Universidad San Francisco de Quito, Colegio de Ciencias e Ingenierías.

Nasar, A., & Mashkoor, F. (2019). Application of polyaniline-based adsorbents for dye removal from water and wastewater—a review. *Environmental Science and Pollution Research,* DOI:10.1007/s11356-018-3990-y

Nasar, A., & Shakoor, S. (2017). Remediation of dyes from industrial wastewater using low-cost adsorbents. In: Inamuddin, Al-Ahmed (Eds.). Applications of adsorption and ion exchange chromatography in waste water treatment. *Materials Research Forum LLC*, Millersville, pp.1-33.

Ritchie, H. & Roser, M. (2019). Water use and sanitation. *Our World in data*. Retrieved from: https://ourworldindata.org/water-use-sanitation

Santillán, P. (2017). Synthesis of porous BiFeO3 materials and their application in water treatment reactions. Tesis (Ingeniería Ambiental). Universidad San Francisco de Quito, Colegio de Ciencias e Ingenierías.

Saravanan, R., Gracia, F. & Stephen, A. (2017). Basic Principles, Mechanism, and Challenges of Photocatalysis. *Springer Series on Polymer and Composite Materials*, 19-40. DOI: 10.1007/978-3-319-62446-4_2

Soltani, T. & Enterazi, M. (2013). Sono-synthesis of bismuth ferrite nanoparticles with high photocatalytic activity in degradation of Rhodamine B under solar light irradiation. *Chemical Engineering Journal*, 223, 145-154

Song, J., Jin, D., Yan, X., Yu, S. & Cheng, J. (2009). Synthesis and Characterization of Porous $BiFeO_3$ Nanoparticles via a Pluronic P123-Assited Sol-Gel Method. *IEEE International Symposium on the Applications of Ferroelectrics*. DOI: 10.1109/ISAF.2009.5307613

Srinivasan, N., Majumdar, P., Eswar, N. & Bandyopadhyaya, R. (2015). Photocatalysis by morphologically tailored mesoporous silica (SBA-15) embedded with SnO2 nanoparticles: Experiments and model. *Applied Catalysis A: General*, 498, 107–116. DOI: 10.1016/j.apcata.2015.03.015

Tamuri, A., Sahar, M., Bakar, N., Lani, M., Kundel, M. & Daud, Y. (2013). Ultraviolet (UV) Light Spectrum of fluorescent lamps. *The Proceedingd of 8th SEATUC Symposium*. DOI: 10.13140/2.1.3114.6886

World Health Organization (WHO). (2009). Concise International Chemical Assessment Document 67. Selected alkoxyehtanols: 2-Methoxyethanol.

World Population Review. (2019). 2019 World Population by Country. Retrieved from: http://worldpopulationreview.com/

World Water Assessment Programme (WWAP). (2018). The United Nations world water development report 2014: nature-based solutions for water. *UNESCO*, ISBN:978-92-3-100264-9

Worldometers. (2019). Water consumption statics. Retrieved from: http://www.worldometers.info/water/

Yanoh, T., Kurokawa, A., Takeuchi, H., Yano, S., Onuma, K., Kondo, T., Miike, K., Miyasaka, T., Mibu, K. & Ichiyanagi, Y. (2014). Characterization of Magnetic and Dielectric Properties of Bi1−xGdxFeO3 Nanoparticles by Local Structure Analyses. *Journal of Nanoscience and Nanotechnolog*y, 14(3), 2190–2197. DOI: 10.1166/jnn.2014.8539

Zhang, N., Chen, D., Niu, F., Wang, S., Qin,L. & Huang, Y. (2016). Enhanced visible light photocatalytic activity of Gd-doped BiFeO3 nanoparticles and mechanism insight. *Scientific Reports* 6, Article number: 26467. DOI: 10.1038/srep26467

Zhao, D.Y., Feng, J.L., Huo, Q.S., Melosh, N., Fredrickson, G. H., Chmelka, B.F. & Stucky, G.D. (1998). Triblock Copolymer Syntheses of Mesoporous Silica with Periodic 50 to 300 Angstrom Pore. *Science,* V. 279, pp. 548-552, DOI: 10.1126/science.279.5350.548